MedChemComm

Accepted Manuscript

ROYAL SOCIETY OF CHEMISTRY

www.rsc.org/medchemcomm

Combretastatin A-4 Inspired Novel 2-Aryl-3-arylamino-imidazo-pyridines/pyrazines as Tubulin Polymerization Inhibitors, Antimitotic and Anticancer Agents

Nitesh Sanghai,[a] Vaibhav Jain,[b] Ranjan Preet,[c] Somnath Kandekar,[a] Sarita Das,[c] Neha Trivedi,[b] Purusottam Mohapatra,[c] Garima Priyadarshani,[a] Maneesh Kashyap,[a] Dipon Das,[c] Shakti Ranjan Sathapathy,[c] Sumit Siddharth,[c] Sankar K. Guchhait,[a] Chanakya N. Kundu,*[c] and Prasad V. Bharatam[a,b]*

[a]Department of Medicinal Chemistry, National Institute of Pharmaceutical Education and Research (NIPER), Sector 67, S. A. S. Nagar (Mohali), Punjab–160062, India

[b]Department of Pharmacoinformatics, National Institute of Pharmaceutical Education and Research (NIPER), Sector 67, S. A. S. Nagar (Mohali), Punjab–160062, India

[c]School of Biotechnology, KIIT University, Campus–11, Patia, Bhubaneswar, Odisha–751024, India

Corresponding Authors*
For S.K.G.: phone, +91 (0)172 2214683; fax, +91 (0)172 2214692;
E-mail, skguchhait@niper.ac.in.
For C.N.K.: phone, +91 (0)674 2725466; fax, + 91 (0)674 2725732;
E-mail, cnkundu@gmail.com.

Graphical Abstract

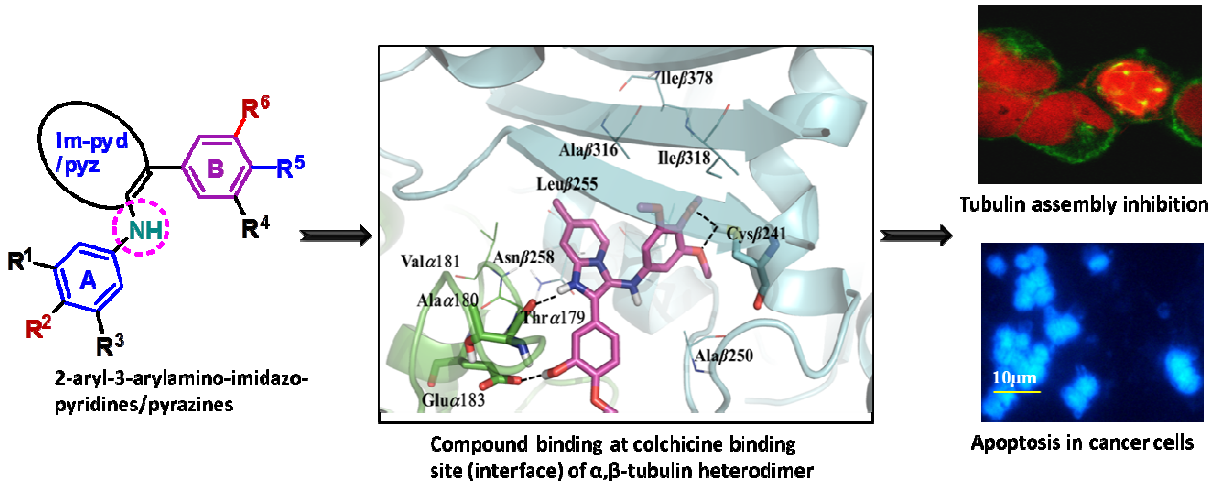

Abstract

Based on the pharmacophoric features of the natural product combretastatin A-4 (CA-4) and its synthetic analogues that inhibit tubulin polymerization, a series of novel 2-aryl-3-arylamino-imidazo-pyridines/pyrazines as potential antitubulin anticancer agents were designed. They were synthesized by a one-pot method involving preparation of isocyanides from the anilines via formylation and subsequent dehydration followed by their reactions with heterocyclic-2-amidines and aldehydes. Compounds **1**, **2**, **14**, and **15** were found to exhibit significant tubulin polymerization inhibition and disruption of tubulin-microtubule dynamics similar to that of CA-4. They showed potent anticancer activities in kidney, breast and cervical cancer cell lines, and relatively low toxicity to normal cells, compared to CA-4. The compounds induced DNA and chromosomal damage, and apoptosis via cell cycle arrest in the G2/M phase. The molecular docking and molecular dynamics (MD) simulation studies revealed that disruption of microtubule dynamics might occur by interaction of the compounds at the colchicine binding site at the interface of α,β-tubulin heterodimer, similar to that of CA-4. Molecular modelling analysis showed that two of the three methoxy groups at ring **A** of all the four potent compounds (**1**, **2**, **14**, and **15)** were involved in bifurcated hydrogen bonding with Cysβ241, an important molecular recognition interaction to show tubulin inhibitory activity. In comparison to CA-4, the bridging NH and the imidazo-pyridine/pyrazine moieties in the title compounds provide flexibility for attaining the required dihedral relationship of two aryls and additional pharmacophoric features required for the interaction with the key residues of the colchicine binding site.

Keywords: Combretastatin, Imidazo-pyridine, Imidazo-pyrazine, Antitubulin, Antimitotic, Anticancer, Molecular Docking, Molecular Dynamics Simulation

Introduction

Microtubules are cytoskeletal filaments composed of α,β-tubulin heterodimer assembly.[1] Their polymerization-depolymerization dynamics are involved in various cellular processes like mitotic spindle formation during cell division, migration, cell shape organization, and transportation of vesicles and mitochondria.[1,2] Agents that disrupt tubulin-microtubule dynamics induce mitotic arrest and eventually cell death by apoptosis.[3,4] Marketed anticancer drugs that target such dynamics are *Catharanthus* (*Vinca*) alkaloids (vincristine, vinblastine and vinorelbine), taxanes (paclitaxel and docetaxel), and epothilones.[5,6] Therefore, tubulin is considered as an important target in anticancer drug discovery research.[3,7-9]

Three binding sites are present in tubulin; the taxane-binding site, the vinca-binding site, and the colchicine binding site.[10,11] Ligands that target the taxane binding pocket act as microtubule stabilizing agents preventing depolymerization,[12,13] whereas agents that interact at the vinca or the colchicine binding sites inhibit the assembly of the α,β-tubulin towards polymerization.[14] Natural ligands that interact at the colchicine binding site include colchicine, steganacin, podophyllotoxin, and combretastatins. They possess similar structural scaffolds, biaryl (for colchicine and steganacin), 1,1-diarylmethane, and 1,2-diarylethene, respectively (Fig. 1). Among combretastatins, CA-4 exhibits pronounced antitubulin cytotoxic effects.[15,16] It specifically interacts at the interface of α,β-tubulin heterodimer and interferes with the flipping in and out of the β-tubulin loop, which in turn prevents the transition from curved to straight heterodimer required for the formation of microtubule assembly.[6,17] Certain agents that bind to the colchicine binding site also lead to tumour vascular disruption.[18-25] CA-4 suffers from poor aqueous solubility, low bioavailability, and short biological half life.[26] To overcome these limitations, various derivatization and formulations of CA-4 have been explored in the last

decade.[27-35] The prodrugs, combretastatin A-4 3-*O*-phosphate (CA-4-P, Zybrestat), combretastatin A-1 2,3-*O*-diphosphate (CA-1-P, OXi4503), and amino acid analogue of CA-4 (AVE8062) are currently in clinical trials.[19,36,37]

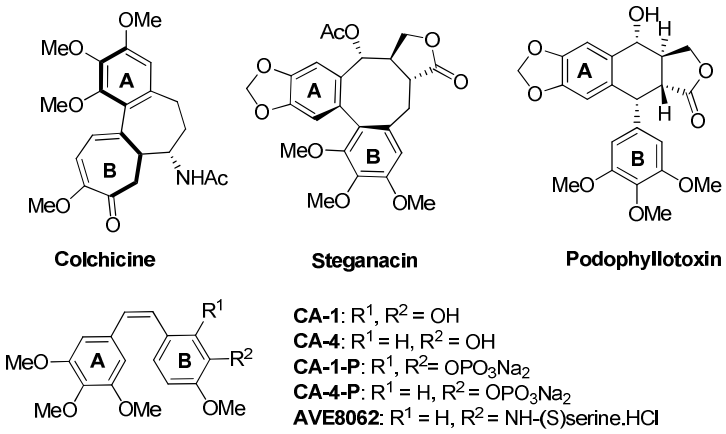

Fig. 1 Natural products that target the colchicine binding site and possess structural resemblance: Combretastatins A-1 and A-4; their (di)phosphates and amino acid analogue prodrugs are in clinical trials.

The important pharmacological features and structural simplicity of CA-4 have made it an attractive lead compound for the development of novel antitubulin anticancer agents. From the structure-activity relationship studies of CA-4, it has been evident that the 3,4,5-trimethoxy substitutions on the ring **A**, 4-methoxy group on ring **B** and a cis configuration between rings **A** and **B** are pharmacophoric requirements for the optimal tubulin inhibitory activity/cytotoxicity.[26,30,38-40]

The 3-hydroxy group in ring **B** is amenable for isosteric replacement or further derivatization for conjugation.[41,42] A study of cis and trans-stilbenes related to CA-4 showed that cis-stilbene configuration provided optimal activity.[43] The stilbenoid structure of CA-4 makes it liable to isomerisation from less stable cis to more stable but inactive trans isomer. This isomerisation is triggered by light, heat and protic media and thus reduces its therapeutic

efficacy.[15,44] The in vitro study of metabolic stability of CA-4 revealed its susceptibility for *Z-E* isomerization of the double bond.[45] Isomerization of cis to trans form can be prevented by locking the cis-type bridge between the two aryl rings. With this perspective, numerous cis-locked analogues of CA-4 with the incorporation of various heterocyclic, carbocyclic, and functional bridging groups as double bond replacements have been explored (Fig. 2).[30,38,43,46-49] A wide range of heterocyclic bridges have been investigated; they include pyrazoles, thiazoles, triazoles, tetrazoles, oxazoles, imidazoles, furans, furanones, furazans, dioxolanes, thiophenes, and indoles.[33,48-50] Carbocyclic moieties that replace double bond are cyclopropane,[51] and cyclopentane.[48,52] The functional bridging groups involve ethers, ketones, sulfonamides, sulfonates, amines, and amide.[53] Recently, pharmacomodulation strategies for the design of potent CA-4 analogues are reported by using introduction of *β*-lactam ring[44,54,55] and isocombretastatin.[56,57]

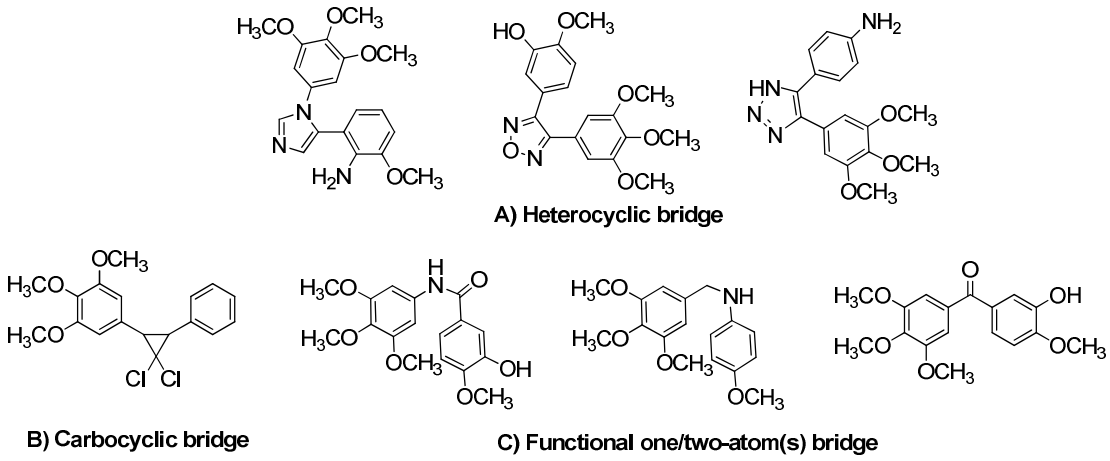

Fig. 2 A few representative analogues of CA-4 replacing double bond with A) heterocyclic, B) carbocyclic, and C) functional bridging moieties.

As a part of our program aimed at natural product based anticancer drug discovery,[58] we were interested in exploration of novel antitubulin anticancer agents and envisaged CA-4

inspired novel 2-aryl-3-arylamino-imidazo-pyridines/pyrazines as potential tubulin polymerization inhibitors (Fig. 3).[50,59-62]

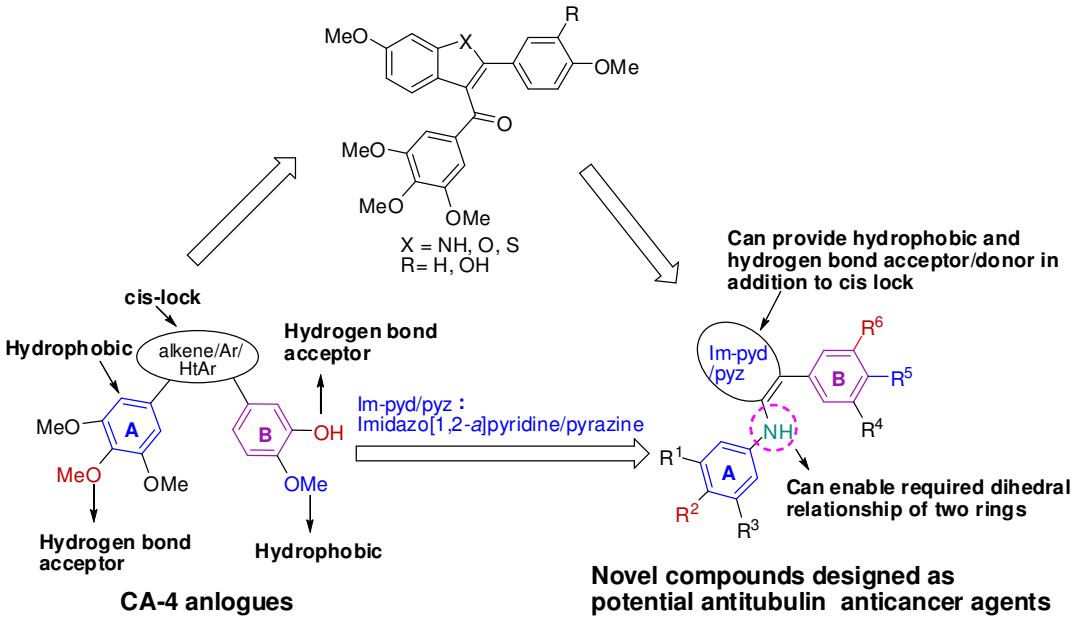

Fig. 3 Design of novel 2-aryl-3-arylamino-imidazo-pyridines/pyrazines as potential antitubulin anticancer agent.

These compounds possess imidazo-pyridine/pyrazine ring as double bond replacement to lock cis-conformation of rings **A** and **B**. Imidazo[1,2-*a*]-pyridine/pyrazine is a class of scaffold present in several marketed drugs and many bioactive compounds.[63-65] Therefore, its incorporation could afford, along with cis-lock, favourable physicochemical properties, improved pharmacokinetic profiles, and additional hydrogen bond donor/acceptor points as well as hydrophobic interactions with α,β-tubulin heterodimer. It has been established that for effective interaction at colchicine binding site in tubulin, CA-4 class of compounds require two phenyl rings to be tilted to each other at a particular range of dihedral angles (around 45º - 55º).[66,67] Natural products colchicine, podophyllotoxin, steganacin, and combretastatins also possess similar dihedral relationships between rings **A** and **B**. 2-Aryl-3-aroyl-

indoles/benzofurans/benzothiophens have been reported as potent inhibitors of tubulin polymerization.[50,60,62] Considering these, we therefore speculated that in our designed compounds also the NH unit could provide flexibility for spatial orientation of two aromatic rings **A** and **B** in the colchicine binding site of *α*,*β*-tubulin heterodimer.

In this article, we present the synthesis, bio-evaluation, and molecular modelling studies of CA-4 inspired novel 2-aryl-3-arylamino-imidazo-pyridines/pyrazines (**1**-**20**). The synthesized compounds were tested *in vitro* and *ex vivo* for their tubulin assembly inhibitory activities, anticancer activities in kidney, breast and cervical cancer cells, and cytotoxicity towards normal cells. The activities were compared with CA-4 and a clinically used anticancer drug 5-fluorouracil. Various biochemical and immunological studies like DAPI (4', 6–diamidino–2–phenylindole) nuclear staining, expression of representative apoptotic protein markers (caspase–3, PARP cleavage, and p53), caspase staining (immunocytochemistry), comet assay, and cytokinesis-block micronucleus (CBMN) assay were carried out to establish the potential of investigated compounds in apoptosis, and damage in DNA as well as chromosomal level. Flow cytometry was also carried out to identify the phase of cell cycle arrest for apoptosis. Furthermore, with an intention of revealing the mode of binding, atomistic level interactions and binding affinity of the title compounds with the *α*,*β*-tubulin heterodimer, molecular docking analysis was carried out on all the investigated compounds. Molecular docking results for the potent antitubulin, anticancer compounds were compared with that of the lead compounds colchicine and CA-4. In addition, molecular dynamics (MD) simulations were also performed on these potent compounds to assess the stability of intermolecular interactions in the dynamical conditions and to estimate the binding free energy of ligands.

Results and Discussion

Chemistry

The 3-aminoimidazo[1,2-*a*]pyridine/pyrazine class of compounds are, in general, prepared by an Ugi–type multicomponent reaction (also referred as Groebke–Blackburn–Bienayme reaction)[68-70] of a heterocyclic-2-amidine with aldehyde and isocyanide. Versatile aldehydes are known to undergo this reaction and can generate substitution diversity at C2 of the product. However, it suffers from the generation of substitution diversity at C3-amine in the scaffold because isocyanides are relatively expensive, unavailable commercially and difficult to prepare.[64,71-73] In our study, the CA-4 inspired novel imidazo-pyridine/pyrazine derivatives required the incorporation of relevant aromatic diversity at C3-amine. A new approach of one-pot preparation of isocyanide directly from amine and its utilization in the Ugi-type reaction was recently developed by our research group.[74] It employs three reactions, formylation of amine, dehydration of formamide to isocyanide, and its reaction with aldehyde and heterocyclic amidine (Scheme 1). The nature of the dehydrating agent and base were found to play a key role in the one-pot process. The method has enabled the incorporation of differently substituted ring **A** at C3-amine and ring **B** at C2 in the products with high yields. The process being one-pot does not require any tedious work-up and purification of any of the intermediates, and minimizes waste products. Using this methodology, CA-4 inspired imidazo[1,2-*a*]-pyridines and pyrazines, imidazo[2,1-*b*]thiazole, and imidazo[2,1-*b*]benzothiazole analogs (compounds **1**-**20**, Fig. 4) with relevant variation at 2-aryl and 3-arylamine were prepared.

Scheme 1. One-pot method for preparation of investigated compounds (**1**-**20**)

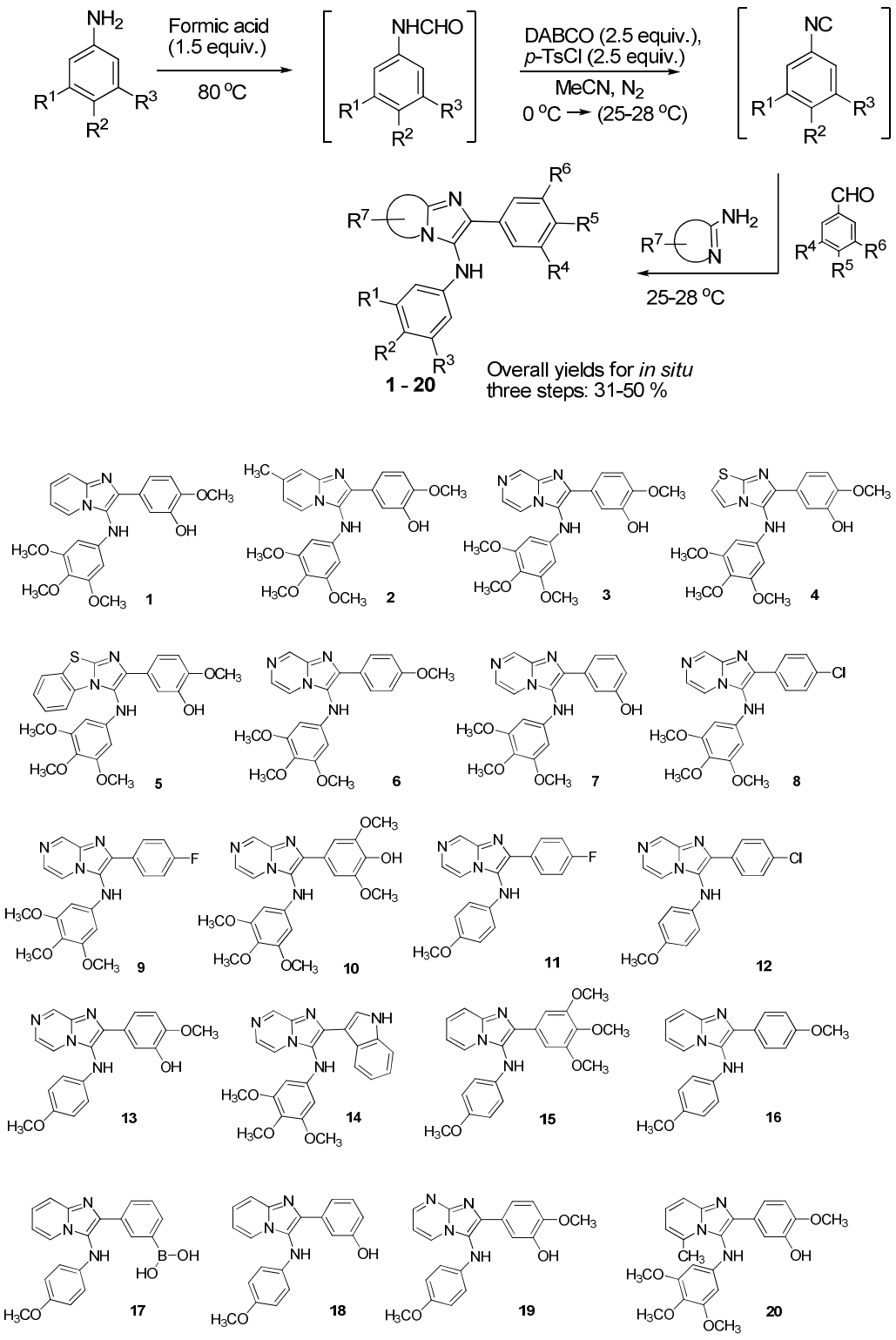

Fig. 4 Synthesized 2-aryl and 3-arylamino substituted imidazo[1,2-*a*]-pyridines and pyrazines, imidazo[2,1-*b*]thiazole, and imidazo[2,1-*b*]benzothiazole analogs (**1**-**20**).

Biological studies

CA-4 inspired imidazo-pyridines/pyrazines inhibit tubulin polymerization and disrupt microtubule dynamics

To study the tubulin polymerization inhibitory activity of novel 2-aryl-3-arylamino-imidazo-pyridines/pyrazines, an *ex vivo* assay in kidney cancer cells (HEK 293T) was performed according to the protocol described under experimental section. All the synthesized compounds (**1**-**20**) were tested with CA-4 as positive control. Interestingly, they were found to possess moderate to good activity of tubulin assembly inhibition (Table 1). The most potent activity was found for compounds **1**, **2**, **14**, and **15** with the IC_{50} (concentration required to inhibit 50% of tubulin assembly) value of 12, 10, 11, and 14 μM, respectively, which were significant in comparison to that of CA-4 (IC_{50}: 9 μM). We were then curious to further confirm the activity of these potent compounds (**1**, **2**, **14**, and **15)** for disruption of tubulin assembly by immunostaining method. HEK 293T cells were treated with these compounds and CA-4 at their respective IC_{50} concentrations and then immunostained with tubulin antibody (Fig. 5). The upper panel represents the tubulin protein assembly of the treated as well as untreated HEK 293T cells labeled with FITC. The middle panel represents the propidium iodide stained nucleus of the cells and the lower panel is the merge of the above two panels. The results imply that the CA-4 and investigated compounds **1**, **2**, **14**, and **15** induced significant distortions in the tubulin assembly of the treated HEK 293T cells leading to the formation of abnormal mitotic spindles in comparison with control. Moreover, investigated compounds showed also significant disruption of tubulin assembly in a similar manner to that of CA-4.

Table 1 IC_{50} of tubulin assembly inhibition using cellular lysate of HEK 293T for investigated compounds and CA-4. Data is the mean ± SD of three different experiments.

Compound	IC_{50} (μM)	Compound	IC_{50} (μM)	Compound	IC_{50} (μM)
1	12 ± 2.0	**8**	32 ± 3.0	**15**	14 ± 2.2
2	10 ± 1.8	**9**	36 ± 1.8	**16**	34 ± 1.5
3	38 ± 2.3	**10**	34 ± 1.7	**17**	48 ± 1.9
4	36 ± 2.1	**11**	44 ± 1.6	**18**	42 ± 3.0
5	20 ± 2.5	**12**	46 ± 2.4	**19**	54 ± 1.8
6	40 ± 2.0	**13**	38 ± 1.8	**20**	38 ± 2.0
7	39 ± 1.2	**14**	11 ± 2.0	**CA-4**	9 ± 1.2

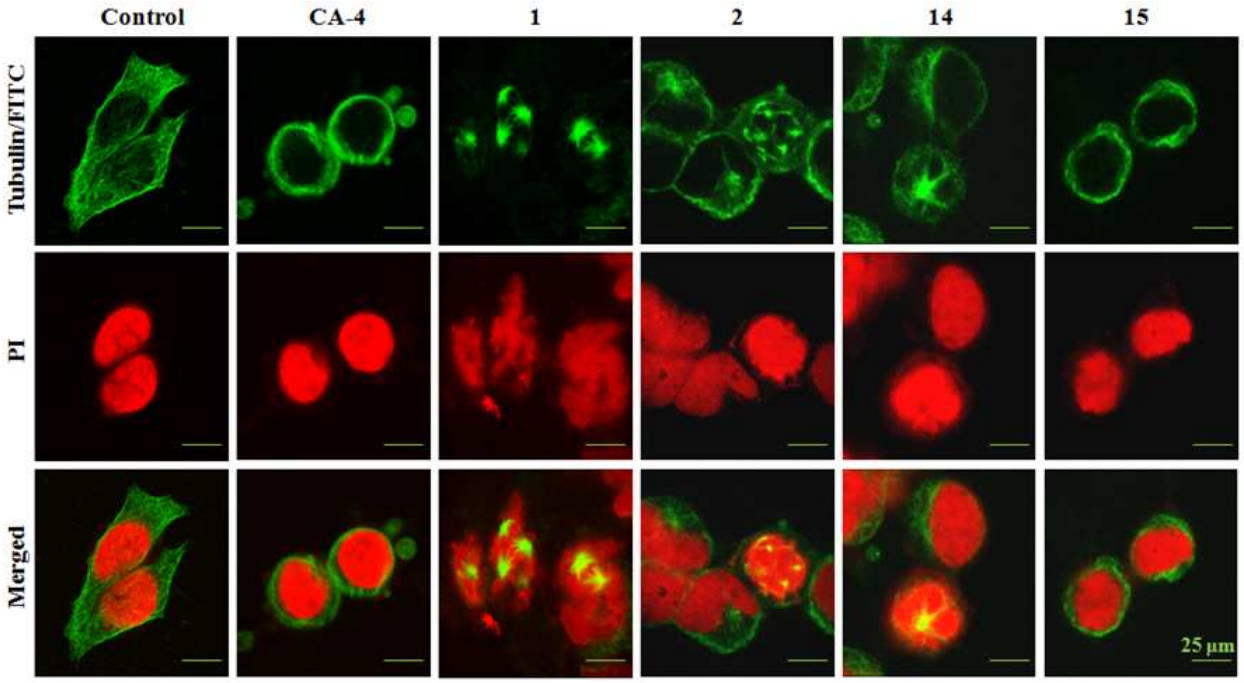

Fig. 5 Immunostaining of tubulin assembly in HEK 293T cells. The upper, middle and lower panels represent the tubulin assembly stained with FITC, the propidium iodide and the merge of above panels, respectively. Images were taken under confocal microscope (Leica TCS SP5). Micrographs presented here is the best of three individual experiments.

Cytotoxic activities of 2-aryl-3-arylamino-imidazo-pyridines/pyrazines

MTT assay was carried out to investigate the cytotoxic activity of all synthesized 2-aryl-3-arylamino-imidazo-pyridines/pyrazines (**1**-**20**) in both kidney cancer cells (HEK 293T) and its

corresponding normal cells (Vero). CA-4 was used as a positive control in the assay. Cells were treated with investigated compounds and CA-4 of increasing concentrations and the viability was measured in concentration dependent manner according to the protocol described under experimental section. It was noted that compounds **1**, **2**, **14**, and **15** resulted in 50% cell death (LC_{50}) in HEK 293T cells at relatively lower concentrations (10, 8, 12, and 10 μM, respectively) than other compounds and 50% cell death in Vero cells at higher concentrations viz. 50, 48, 70, and 65 μM, respectively (Table 2 and Fig. S1). Thus, these results demonstrated that the compounds **1**, **2**, **14**, and **15** are more potent cytotoxic agents than other tested compounds and posses significant cytotoxicity in HEK 293T, but less cytotoxicity for Vero cells. To further extend the cytotoxic potential of CA-4 and the investigated compounds, we have measured cytotoxicity in a panel of cell lines with different time points (24 h and 48 h) of treatment (Table 3). The data showed that SiHa and HeLa (cervical cancer cell lines) were more susceptible to CA-4 in comparison to MCF-7 and HEK 293T cells. To measure the anti-colony forming potential of the compounds against a single cell towards formation of a colony or clone in long term, a widely used clonogenic cell survival assay was performed. It was noticed that compounds **1**, **2**, **14** and **15** showed significant reduction in colony formation in HEK 293T cells (Fig. S2). The investigated compounds (**1**, **2**, **14** and **15**) showed also significant anchorage dependent anti-cell migration potential in HEK 293T cells (Fig. S3). Interestingly, these cytotoxicity results were in accordance with the tubulin polymerization inhibitory activities of the investigated compounds and CA-4. This indicates the disruption of tubulin-microtubule dynamics as a major pathway for cytotoxic properties of the investigated 2-aryl-3-arylamino-imidazo-pyridines/pyrazines class of compounds.

Table 2 LC_{50} values (μM) of CA-4 and investigated compounds (**1**-**20**) for kidney cancer cells (HEK 293T) and its corresponding normal cells (Vero).

Compound	LC_{50} (Vero)	LC_{50} (HEK 293T)	Compound	LC_{50} (Vero)	LC_{50} (HEK 293T)
1	50 ± 2.0	10 ± 1.0	**12**	45 ± 2.0	34 ± 1.8
2	48 ± 3.0	8 ± 0.5	**13**	62 ± 2.5	38 ± 2.4
3	50 ± 2.3	38 ± 2.0	**14**	70 ± 1.6	12 ± 0.6
4	62 ± 2.5	36 ± 3.0	**15**	65 ± 2.0	10 ± 0.3
5	26 ± 2.0	22 ± 2.1	**16**	54 ± 1.6	34 ± 2.0
6	75 ± 2.4	54 ± 2.2	**17**	58 ± 2.4	48 ± 1.9
7	63 ± 1.6	42 ± 2.3	**18**	74 ± 3.0	47 ± 2.6
8	32 ± 2.7	25 ± 2.2	**19**	56 ± 1.6	54 ± 1.8
9	48 ± 1.9	36 ± 1.7	**20**	74 ± 2.2	63 ± 2.0
10	62 ± 1.5	34 ± 2.0	**CA-4**	11 ± 0.5	8 ± 0.6
11	72 ± 2.0	56 ± 2.5			

Table 3 LC_{50} values (μM) of CA-4 and investigated compounds (**1**, **2**, **14**, and**15**) against various cancer cells with different time of treatment.

Compound	SiHa (μM)		MCF-7 (μM)		HEK-293T (μM)		HeLa (μM)	
	24 h	**48 h**	**24 h**	**48 h**	**24 h**	**48 h**	**24 h**	**48 h**
CA-4	0.6 ± 0.02	0.2 ± 0.01	7 ± 1	2 ± 0.8	8 ± 1	0.2 ± 0.01	6 ± 1	0.8 ± 0.2
1	5 ± 1	2 ± 0.1	20 ± 2.3	12 ± 1	10 ± 1	5 ± 1	15 ± 2.1	10 ± 1
2	4 ± 1	1.5 ± 0.1	15 ± 2	10 ± 1	8 ± 2	3 ± 1.4	15 ± 2	7 ± 1
14	7 ± 1	3 ± 0.9	18 ± 1.5	6 ± 1	12 ± 2	3 ± 1.2	17 ± 2	9 ± 1
15	5 ± 1.2	2 ± 0.9	8 ± 1	5 ± 1	10 ± 2	5 ± 1	9 ± 1	5 ± 1

Determination of phase of the cell cycle arrest in kidney cancer cells

To investigate the regulation of cell cycle profile in HEK 293T cells, fluorescence activated cell sorter (FACS) analysis was carried out. The cells were treated with CA-4 and the compounds **1**, **2**, **14**, and **15** for 24 h, stained with propidium iodide (PI), and then FACS analysis was performed. The DNA content was measured at each phase of the cell cycle and the data is represented in Fig. S4. It was observed that all the four compounds induced cell cycle arrest in

G2/M phase, which is in accordance to that of CA-4 and tubulin polymerization inhibition property.

Apoptotic effect of the compounds 1, 2, 14, and 15 in kidney cancer cells

A nuclear staining experiment using HEK 293T cells was performed to investigate the apoptotic effect of 2-aryl-3-arylamino-imidazo-pyridines/pyrazines **1**, **2**, **14**, and **15.** Chromatin condensation and nuclear fragmentation of the cancer cells was analyzed by fluorescence microscopy using the DNA-binding fluorescent dye DAPI after treating the cells with the investigated compounds and CA-4 at their respective LC_{50} concentrations for 24 h using a protocol as described in experimental section. It was observed that the chromatin condensation and nuclear fragmentation increased significantly in the treated cells in comparison to untreated cells (control) that suggested the presence of apoptotic nuclei (Fig. 6A). The apoptotic nuclei resulted in the cancer cells treated with the investigated compounds increased substantially in comparison with the untreated cells and was comparable to that of CA-4 (Fig. 6B). To further corroborate the apoptotic effect of the compounds in HEK 293T cells, the expression level of representative apoptotic marker proteins such as p53, PARP and its cleaved products was studied (Fig. 6C). In the experiment, GAPDH was used as loading control. In comparison with the untreated cells, treated cells showed a significant increase in the expression of p53 and the level of cleaved products (86 kDa) of PARP, and reduced level of full length (116 kDa) of PARP. These results indicate that the investigated compounds possess apoptotic effect in HEK 293T cancer cells. To examine whether the induction of apoptosis by the investigated compounds is associated with the activation of caspase-3, an immunocytochemical assay was performed. The results indicate that the investigated compounds activate caspase-3 in HEK 293T cells (Fig. S5).

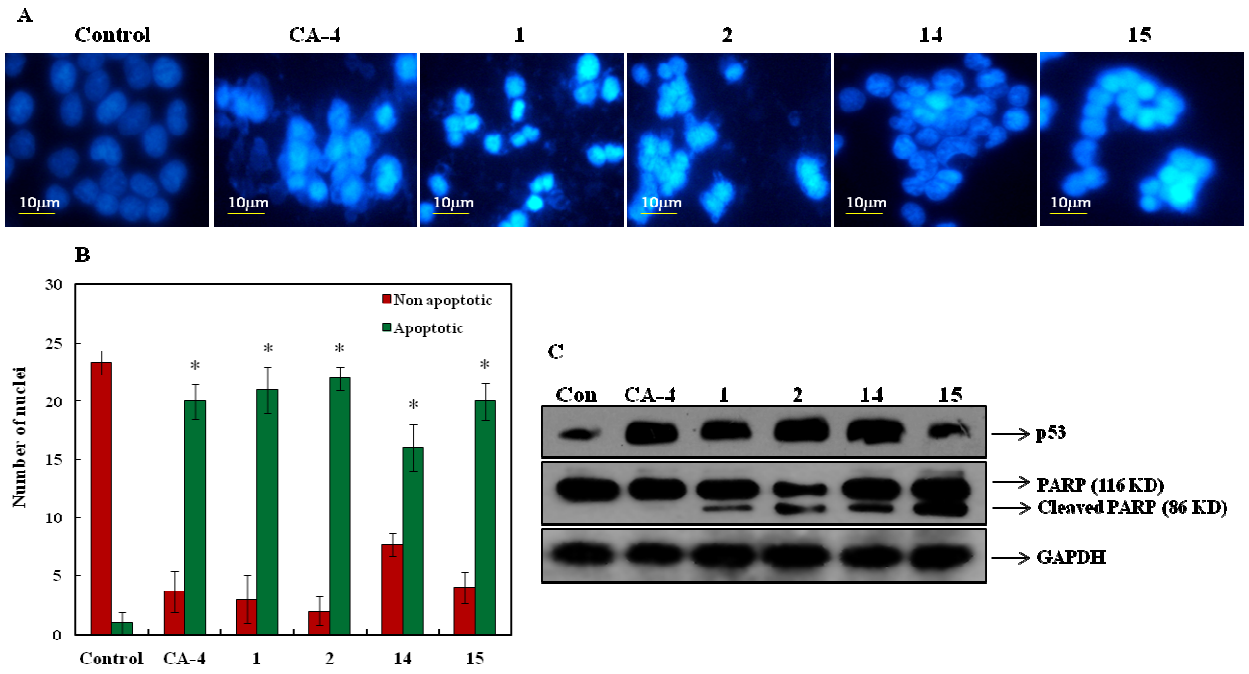

Fig. 6 CA-4 and the investigated compounds **1**, **2**, **14**, and **15** induce apoptosis in HEK 293T cells. **(A)** DAPI nuclear staining experiment: Images were taken using fluorescent microscope (Nikon, Japan) at 40X magnification. Images represented here are one of the replicates of three different experiments. **(B)** A graphical representation of apoptotic nuclei of (A) (**P*<0.05). The red and green bars represent the non-apoptotic and apoptotic nuclei, respectively. **(C)** Western blot analysis showing the expression level of p53, and PARP and its cleaved products in HEK 293T cells. GAPDH was used as loading control.

Compounds induce DNA and chromosomal damage

To determine whether the investigated compounds contribute to DNA damage, a well known comet assay was performed. The HEK 293T cells were treated with CA-4 and the compounds **1**, **2**, **14**, and **15** at their respective LC_{50} concentrations for 24 h and then the comet assay was carried out according to the protocol described in experimental section. In treated cells, there were lesions in DNA and the comet lengths were increased drastically, while no comet formation was seen in untreated cells (Fig. S6A). The bar diagram shown in Fig. S6B represents the comet lengths in pixels. From these data, it appears that the investigated compounds cause DNA damage in kidney cancer cells. Further, to examine whether CA-4 and the investigated

compounds have potential to cause damage at chromosomal level, a cytokinesis-block micronucleus (CBMN) assay was performed. Micronuclei originate from the chromosome fragments or whole chromosomes that lag behind at anaphase during nuclear division. CBMN assay has evolved into a comprehensive method for measuring chromosome breakage, DNA miss-repair, chromosome loss, necrosis, apoptosis, and cytostasis.[75] The HEK 293T cells were treated with CA-4 and the investigated compounds at their LC_{50} concentrations and then CBMN assay was performed. It was observed that micronuclei formed in treated cells, whereas no micronuclei formation was seen in untreated cells, indicating the chromosomal damage (Fig. S6C). Therefore, these results confirm that the CA-4 and the investigated compounds not only induce DNA damage but also the chromosomal damage simultaneously.

Molecular Docking analysis

Molecular docking has emerged as one of the very robust and efficient approaches for understanding the interaction between macromolecules and small molecules, which further leads to the rationalization of lead optimization efforts. In the past, several molecular modeling studies[76] like ligand-based pharmacophore mapping,[66,77] molecular docking,[78-80] and virtual screening[81,82] have been performed by various research groups on antitubulins acting on colchicine binding site. These studies revealed an insight into the atomistic level details of ligands interacting with α,β-tubulin heterodimer, their binding affinity and important pharmacophoric features necessary for inhibition of microtubule assembly. Based on the important pharmacophoric features considered in the design of the investigated compounds, it is obvious to speculate that the compounds can interact at the colchicine binding site of tubulin similar to that of CA-4. Accordingly, molecular docking studies were performed to investigate the binding pose, intermolecular interactions and binding affinity of ligands with the α,β-tubulin

heterodimer. The docking results of four potent compounds (**1**, **2**, **14,** and **15**) are discussed herein; the results of all investigated compounds (**1**-**20**) have been provided in Table S1 (supporting information). Moreover, the interaction profile and docking score of the potent compounds were also compared with that of colchicine and CA-4 (for molecular docking analysis of colchicine and CA-4, see supporting information, Fig. S7, Fig. S8).

Docking of potent 2-aryl-3-arylamino-imidazo-pyridines/pyrazines

The result of the ligands preparation in Ligprep module of Schrödinger molecular modeling package[83] showed that 2-aryl-3-arylamino-imidazo-pyridines/pyrazines at pH 7 ± 2 can exist in two different charged states (predicted by Epik program), protonated (charge +1, protonation occurs at N1 nitrogen of imidazole ring) and neutral (charge 0). Further, to identify the most plausible charged state of these species in terms of their stability, potent compounds (**1**, **2**, **14,** and **15**) were subjected to quantum chemical calculations using density functional theory (DFT) method at B3LYP/6-31+G(*d,p*) level by GAUSSIAN03 programme.[84] This analysis suggested that the calculated protonation energy for these compounds falls in the range of 237-245 kcal/mol (Table S2, supporting information), which is quite favourable and thus they prefer to exist in protonated form. Further, the pk_a value (~7.1) of imidazole nitrogen predicted by ChemAxon MarvinView software[85] corroborated that the compounds are basic in nature. Therefore, the docking results for the protonated state of these compounds are presented in this work (Table 4). In order to see the differences in the docking scores and intermolecular interactions of neutral species (**1**-**20**), they were also docked into the colchicine binding site of tubulin and the results are shown in Table S3 (supporting information). Minor variation in the docking score and interactions in comparison to protonated state were observed for the neutral state compounds.

Docking of the potent investigated compounds (**1**, **2**, **14,** and **15**) into the colchicine binding site of *α,β*-tubulin heterodimer (Fig. S9) revealed that the major portion of these compounds was buried in the *β*-subunit (showing maximum interactions) and a fewer interactions with residues of *α*-subunit, colchicine and CA-4 (Fig. 7 and Fig. S9). The binding pose and interactions for CA-4 and investigated compounds **1**, **2**, and **14** revealed that imidazo-pyridine/pyrazine in the compounds can mimic the 3-hydroxy-4-methoxyphenyl moiety of CA-4 (see Fig. S10 for superimposition). This is an important observation in the aspect that the 3-hydroxy-4-methoxyphenyl moiety in the CA-4 or its cis-locked analogues can be replaced by a suitable heterocycle moiety such as imidazo-pyridine/pyrazine for retaining antitubulin activity. The Glide docking scores for the potent compounds **1**, **2**, **14**, and **15** (-9.33, -10.02, -8.82 and -8.59, respectively) were comparable to that of known tubulin inhibitors colchicine (-10.19) and CA-4 (-8.38) (Table 4). In addition, intermolecular interactions (hydrogen bonding, hydrophobic, C-H$\cdots\pi$ and N-H$\cdots\pi$) of the docked potent compounds were found to be consistent with the binding model of colchicine and CA-4. These results are in agreement with the tubulin polymerization inhibitory assay which showed that the potent compounds **1**, **2**, **14**, and **15** (IC_{50}: 12, 10, 11 and 14 μM, respectively) have comparable activity to that of CA-4 (IC_{50}: 9 μM). The methoxy group of all the potent compounds showed bifurcated hydrogen bonding with Cys*β*241, an essential interaction to show tubulin inhibition activity.[76] Moreover, protonated nitrogen (N1) of imidazo-pyridine/pyrazine ring of compounds **1**, **2,** and **14** formed hydrogen bonding with the main chain carbonyl of Thr*α*179, whereas in compound **15** bridging NH showed relatively weaker hydrogen bonding with the same residue (distance 3.74 Å). This is due to the lack of flexibility between ring **A** and imidazo[1,2-*a*]-pyridine ring of compound **15**, which flips the orientation of ring **B** inside the binding site in comparison to other three compounds. The

dihedral angle between ring **A** and imidazo-pyridine/pyrazine ring of compounds **1**, **2** and **14** was found to be 46.70°, 49.93° and 51.92°, respectively, while for compound **15** the dihedral angle between rings **A** and **B** was 48.90°. Therefore, this endorses further the reported studies [66,67] that optimum range of dihedral angle is necessary between the aryl rings for the compounds to bind at colchicine site of the tubulin. This also signifies the importance of bridging NH in providing the flexibility to the title compounds for showing maximum interactions with the *α,β*-tubulin heterodimer. The imidazo-pyridine/pyrazine ring of all the four potent compounds were also found to be involved in N-H· · ·π (except compound **15**) and hydrophobic interactions with the residues of the colchicine binding site, implying the significance of the heterocyclic scaffold considered in the title compounds.

The binding model of the best docked compound **2** (Glide score -10.19) showing interactions with the tubulin heterodimer is depicted in Fig. 7. In detail, methoxy groups of compound **2** formed key interaction with the side chain -SH of Cys*β*241 (hydrogen bond distance 1.84 Å and 2.42 Å). In addition, the 3-hydroxyl group of compound showed hydrogen bond with the side chain carboxyl group of Glu*α*183 (2.01 Å) and protonated nitrogen of imidazole ring formed hydrogen bond with the main chain carbonyl of Thr*α*179 (2.41 Å) (not present in the unprotonated form of compound), which is further providing stability to the protein-ligand complex. Other residues like Val*α*181, Ala*α*180, Leu*β*242, Ala*β*250, Ala*β*316, Ile*β*318 and Ile*β*378 were found to be involved in hydrophobic interactions, while some other weaker contacts like CH· · ·π interaction with Leu*β*255 and NH· · ·π interaction with Asn*β*258 were also observed for compound **2**. Molecular docking of other investigated compounds **1**, **14**, and **15** showed almost similar intermolecular interactions as those of compound **2**, CA-4, and colchicine. This molecular docking study indicates that the title compounds have strong potential

to bind at the interface of *α,β*-tubulin heterodimer, which in turn destabilize/inhibit the tubulin polymerization as observed in the experimental study.

Table 4 Comparison of molecular docking results (Glide score and non-bonding interactions) of known tubulin inhibitors colchicine and CA-4 with the potent investigated compounds (sorted according to Glide score). Value 2 in parenthesis of column 4 indicates the bifurcated hydrogen bond.

Compound	Glide Score	Hydrogen Bonding interaction		Hydrophobic interaction	C-H· · ·π interaction	N-H· · ·π interaction
		Backbone	Side chain			
Colchicine (Charge 0)	-10.19	Val*α*181	Cys*β*241(2)	Ala*α*180,Leu*β*242, Ala*β*250 Ala*β*316, Ile*β*318, Ile*β*378	Leu*β*255	Asn*β*258
2 (Charge +1)	-10.02	Thr*α*179 (2.41 Å)	Glu*α*183 Cys*β*241(2)	Ala*α*180,Val*α*181, Ala*β*250, Ala*β*316, Ile*β*318, Ile*β*378	Leu*β*255	Asn*β*258
1 (Charge +1)	-9.33	Thr*α*179 (2.63 Å)	Glu*α*183 Cys*β*241(2)	Ala*α*180,Val*α*181, Ala*β*250, Ala*β*316, Ile*β*318, Ile*β*378	Leu*β*255	Asn*β*258
14 (Charge +1)	-8.82	Thr*α*179 (2.85 Å), Asn*β*249	Cys*β*241(2)	Ala*α*180,Val*α*181, Ala*β*250, Ala*β*316, Ile*β*318, Ile*β*378	Leu*β*255	Asn*β*258
15 (Charge +1)	-8.59	Thr*α*179 (3.74 Å)	Cys*β*241(2)	Ala*α*180,Val*α*181, Ala*β*250, Ala*β*316, Ile*β*318, Ile*β*378	Leu*β*255	Asn*β*258
CA-4 (Charge 0)	-8.38	Val*α*181	Cys*β*241(2)	Ala*α*180,Val*α*181, Ala*α*180, Leu*β*242, Ala*β*250, Ala*β*316, Ile*β*318, Ile*β*378	Leu*β*255	Asn*β*258

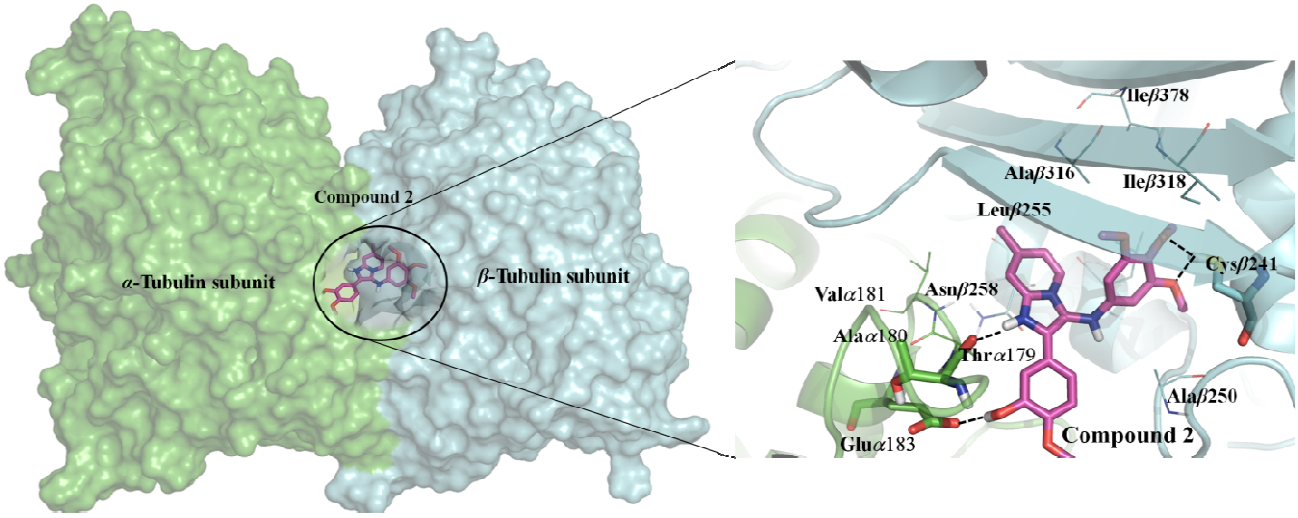

Fig. 7 Binding model of ligands at the interface of *α,β*-tubulin heterodimer. Compound 2 is shown in stick models (*magenta* color). For clarity non-polar hydrogen atoms have been deleted from the ligands. Hydrogen bonding interactions are shown as black dashes, and residues involved are represented also in stick models, while residues involved in other intermolecular interactions are represented as lines. *Green* and *cyan* color represents *α*- and *β*-tubulin, respectively.

Molecular Dynamics (MD) Simulation Analysis

In the previously reported studies, MD simulations were implemented to refine the tubulin-inhibitor complex,[80] calculation of potential energy of tubulin inhibitors in order to identify the correct binding pose,[79] and stability of interactions during the dynamical process to distinguish active from inactive ligand.[86] In another study, constrained molecular dynamics simulation and hydropathy analysis were performed to investigate the reason behind the lower and higher activity of the ligands.[66] In comparison to these MD studies, which run simulation for a few hundreds of picoseconds, the present simulation was performed for long run (10 ns) to get more detailed insight into the stability of *α,β*-tubulin-ligand complex and their intermolecular interactions (special emphasis on Cys*β*241) in dynamical conditions, and to estimate the binding free energy of ligands. All the full atomistic MD simulations were performed using AMBER 11 package.[87] For the purpose of MD simulations, best docking pose of the four potent investigated

compounds (**1**, **2**, **14**, and **15** in their protonated states) and known tubulin inhibitor CA-4 with *α,β*-tubulin heterodimer were selected. Root-mean-square deviation (RMSD) analysis of Cα backbone atoms of protein and all the atoms of ligand throughout the simulation run are provided in the supporting information (Fig. S11).

Hydrogen bond analysis

Hydrogen bonding analysis between protein and ligand was carried out to investigate the stability of these intermolecular interactions under dynamical conditions and to identify the predominant protein residues involved in such type of contacts. Hydrogen bond formation ability of potent compounds (**1**, **2**, **14**, and **15**) and CA-4 analyzed during the last 2 ns of total simulation run is presented in Fig. S12. There is a clear distinction in the number of hydrogen bonds formed by CA-4 and the potent compounds with the residues of *α,β*-tubulin heterodimer in each frame. CA-4 formed only one persistent hydrogen bond throughout the trajectory, while potent investigated compounds showed 1-3 hydrogen bonds. This exemplify that the incorporation of additional pharmacophores (bridging NH and imidazo-pyridine/pyrazine moiety) into CA-4 resulted in enhanced intermolecular interactions.

The contribution of each amino acid residues involved in the hydrogen bonding during the last 2 ns trajectory (1000 frames) was also assessed in terms of their occupancy (Fig. 10). The maximum hydrogen bond occupancy in protein complexed with CA-4 was shown by hydrophobic residue Val*β*315 (9.90%), this residue interacts with the –OH group at ring **B** of the ligand. In case of protein complexed with potent compounds **1**, **2**, **14**, and **15** the highest occupancy was exhibited by residues Ser*α*178 (74.20%), Thr*α*179 (39.60%), Leu*β*248 (37.60%) and Asn*β*249 (26.40%), respectively. It was observed that the protonated nitrogen at imidazole ring of the compounds **1**, **2** and **15** formed hydrogen bonding interactions with the respective

residue showing highest occupancy, whereas in compound **14**, indole ring –NH interacted with the residue exhibiting maximum occupancy. Interestingly, in all the protein-ligand complexes, hydrogen bonding was observed between the side chain -SH of Cysβ241 (critical residue for antitubulin activity) of a protein and oxygen of methoxy groups at ring **A** of the ligands. The hydrogen bond occupancy of Cysβ241 for protein complexed with ligands CA-4, **1**, **2**, **14**, and **15** was found to be 1.70%, 4.60%, 4.60%, 6.40% and 6.70%, respectively. Although, Cysβ241 represent low occupancy (due to stringent criterion of hydrogen bonding) in all the cases but it was always in close proximity to the two of the methoxy oxygens. Being a critical residue in the interaction of tubulin and inhibitors, Cysβ241was analysed for the proximity to methoxy groups of ligands (see supporting information for detailed analysis, Fig. S13). The results indicate that side chain of Cysβ241 is in a distance range close enough to form hydrogen bonds with two of the three ring A methoxy groups.

Binding free energy calculations

The length of a simulation run plays a significant role to obtain the reliable binding free energy estimate of the protein-ligand complex.[88] Therefore, to observe the fluctuations in the binding free energy during the whole simulation run, calculations were initially performed on 100 snapshots of each 1 ns trajectory until 10 ns, using Molecular Mechanics-Generalized Born Surface Area (MM-GBSA) method.[89] The binding free energy with respect to simulation time for the known tubulin inhibitor CA-4 and potent investigated compounds (**1**, **2**, **14**, and **15**) with α,β-tubulin heterodimer are depicted in Fig. S14. It is clearly reflected from the graph that binding free energy gets equilibrated during the last 2 ns of the simulation run i.e. from 9-10 ns. This suggested that simulation time was long enough to study the thermodynamics and energetic contribution of various intermolecular forces within a system.

Based on these results, average binding free energy of ligands for the last 2 ns trajectory is reported in this article (Table 5) along with the contribution of different energy components (van der Waals, electrostatic, polar solvation and nonpolar solvation interaction energies). The binding free energy for the ligands CA-4, **1**, **2**, **14**, and **15** via MM-GBSA was predicted to be -37.57, -40.51, -34.24, -30.95 and -36.87 kcal/mol, respectively. Therefore, in accordance with the *ex vivo* tubulin polymerization inhibitory activities (similar IC_{50}) and molecular docking results (similar Glide score), the binding free energies of the potent compounds are comparable to that of CA-4. Total relative binding free energy (ΔG_{bind}) equals to the sum of gas phase energy (ΔG_{gas}) and solvation free energy (ΔG_{solv}). In case of CA-4, gas phase and solvation free energies were found to be -62.78 and 25.21 kcal/mol, respectively, signifying that the former has favourable and later has unfavourable energetic contribution to the total binding free energy. Likewise, in all the other potent investigated compounds, gas phase energy was favourable (-546 to -596 kcal/mol) while solvation free energy was unfavourable (510 to 562 kcal/mol).

It can also be observed from Table 5 that van der Waals energy of potent compounds (**1**, **2**, **14**, and **15**) is more (about 10-15 kcal/mol) as compared to CA-4, this could be due to the presence of additional hydrophobic imidazo-pyridine/pyrazine ring in the compounds. In addition, electrostatic energy component of compounds (-488 to -532 kcal/mol) was much higher in comparison to that of CA-4 (-14.22 kcal/mol). This difference is attributed to the presence of protonated nitrogen in imidazole ring of compounds, which makes them positively charged and hence can interact with the negatively charged residues of the colchicine binding site. It should also be noted that the formal charge of the α,β-tubulin heterodimer along with GTP is -38.00, implying that the protein is majorly composed of negatively charged residues. Another reason behind the more favourable electrostatic contribution in case of potent compounds than CA-4

may be because of higher hydrogen bond formation ability of former with the residues of protein as compared to later (Fig. S12). Moreover, in all the potent compounds electrostatic energy component is predominant than van der Waals contribution to the overall binding energy, while in CA-4 van der Waals energy is the main driving force behind the stabilization of protein-ligand complex.

Table 5 Average binding free energy results (last 2 ns) for α,β-tubulin-ligand complexes along with its different energy components.[a]

Compound	VDW	EEL	EGB	ESURF	ΔG_{gas}	ΔG_{solv}	ΔG_{bind}
CA-4	-48.56	-14.22	30.77	-5.57	-62.78	25.21	-37.57 ± 2.62
1	-57.10	-494.67	517.60	-6.34	-551.77	511.26	-40.51 ± 4.21
2	-64.60	-531.94	569.52	-7.22	-596.54	562.30	-34.24 ± 4.20
14	-59.98	-484.21	520.14	-6.90	-544.19	513.24	-30.95 ± 3.33
15	-57.81	-488.65	515.81	-6.23	-546.46	509.58	-36.87 ± 3.48

[a] The meaning of the different terms used in this table is as follows: **VDW** = van der Waals energy as calculated by the MM force field. **EEL** = electrostatic energy as calculated by the MM force field. **EGB** = the electrostatic contribution to the solvation free energy calculated by GB. **ESURF** = nonpolar contribution to the solvation free energy calculated by an empirical model. ΔG_{gas} = total gas phase energy i.e. sum of van der Waals and electrostatic energy from MM. ΔG_{solv} = total solvation free energy i.e. sum of electrostatic and nonpolar contributions from solvation. ΔG_{bind} = final estimated binding free energy calculated from the terms above (kcal/mol).

Conclusions

In conclusion, a series of combretastatin A-4 inspired novel 2-aryl-3-arylamino-imidazo-pyridines/pyrazines were designed. They were synthesized by a one-pot approach involving the preparation of isocyanides directly from amines via formylation and subsequent dehydration followed by their reaction with heterocyclic-2-amidines and aldehydes. *Ex vivo* tubulin polymerisation assay and *in vitro* immunostaining experiment revealed that among the investigated compounds (**1**-**20**), compounds **1**, **2**, **14**, and **15** were found to possess significant activities for inhibition of tubulin polymerization and disruption of tubulin-microtubule dynamics, comparable to that of CA-4. MTT and clonogenic assays showed that these compounds exhibited potent anticancer activities in various cancer cell lines (kidney, breast, and cervical), and relatively low toxicity to normal cells, compared to CA-4. Various biophysical and immunological studies including DAPI nuclear staining, expression of representative apoptotic protein markers, immunocytochemistry, comet assay, and cytokinesis-block micronucleus assay implied their good efficacies in apoptosis, and DNA as well as chromosomal damage in HEK 293T cells. Furthermore, flow cytometry indicated that the compounds induced cell-arrest in G2/M phase of cell cycle. Molecular docking and MD simulation studies suggest that these compounds occupied the colchicine binding site at the interface of α,β-tubulin heterodimer, similar to that of CA-4, and stabilized the complex by forming multiple interactions with the key residues (including the important molecular recognition residue Cysβ241) of the protein. Moreover, the compounds showed docking score and binding free energy values comparable to that of CA-4. Interestingly, molecular modeling studies revealed that in comparison to CA-4, the bridging NH and the imidazo-pyridine/pyrazine ring in the title compounds provided additional pharmacophoric features for the inhibition of tubulin polymerization. The bridging NH group

afforded the flexibility in attaining the required dihedral angel between two aryl moieties for maximum binding with tubulin. The protonated nitrogen (N1) of imidazo-pyridine/pyrazine ring showed hydrogen bonding, and also the ring was found to be involved in NH· · ·π and hydrophobic interactions.

In overall, the results of tubulin polymerization inhibition, disruption of microtubule networks, cytotoxic activities, relative potencies, and cell cycle arrest in G2/M phase were found to be in accordance, and supported by *in silico* results of mode of interaction with tubulin. These suggested the inhibition of tubulin polymerization via interacting on colchicine binding site as mode of action for exhibiting cytotoxic and anti-proliferative properties of the investigated compounds. This work will provide impetus in rational structural modulation by considering the important pharmacophoric features of the lead compounds for the identification of novel anticancer agents that can target at colchicine binding site of tubulin. The relevant studies of the investigated potent compounds for their further development are underway.

Experimental Section

Chemistry

General considerations: All reactants and reagents were obtained from commercial source and used without further purification except solvent. The NMR spectra were recorded on a Bruker Avance DPX 400 MHz spectrometer in $CDCl_3$/DMSO–d_6/CD_3OD solvents using TMS as an internal standard. *J* values are given in Hz. Mass spectra were recorded with LCMS–MAT–LCQ [for ESI and APCI], Bruker–Maxis [for HRMS] mass spectrometers. IR spectra were recorded on a Nicolet FT–IR Impact 410 instrument as thin film (neat). The reactions were monitored by TLC (Merck®, Silica gel 60 F_{254}). The purity of synthesized compounds was analyzed by HPLC (Shimadzu LC–6AD system), Phenomenex RP–C18 column (250 x 4.60 mm), particle size 5 μm, flow rate 1mL/min, using water-acetonitrile.

Synthesis of 2-Aryl-3-arylamino-imidazo-pyridine/pyrazine derivatives (1-20)

Representative synthesis of 2-(3-Hydroxy-4-methoxyphenyl)-3-(3,4,5-trimethoxyphenyl-amino)imidazo[1,2-*a*]pyridine (compound 1)

A mixture of trimethoxyaniline (1 mmol) and formic acid (1.5 mmol) was stirred at 80 °C. After completion of reaction (2.5 h), the resultant mixture was cooled to 0 °C and the assembly was flushed with nitrogen. Anhyd. acetonitrile (1.5 mL), DABCO (2.5 mmol, 280 mg) and *p*-TsCl (2.5 mmol, 475 mg) were subsequently added to the mixture at 0 °C under nitrogen. The reaction temperature was allowed to gradually elevate to RT (25–28 ^{o}C) by removing the ice bath and the reaction was continued at RT. To realize the progress of conversion of *N*-formamide to isocyanide, a TLC-monitoring process that can circumvent the pungent smell of isocyanide was performed. A little portion of the reaction mixture was quenched with saturated aqueous solution of $CuSO_4$. The aqueous solution was mini-extracted with EtOAc in a vial and the EtOAc solution

was checked for TLC. After complete conversion of *N*-formamide to isocyanide as indicated by TLC (4 h), 2-aminopyridine (1 mmol) and 3-hydroxy-4-methoxybenzaldehyde (1 mmol) were added. The reaction mixture was heated at 50 °C. The resultant mixture after completion of the reaction as indicated by TLC (16 h) was extracted with EtOAc (2x25 mL). The combined organic solution was washed with water (2x5 mL) and brine (1x5 mL), dried with anhyd. Na_2SO_4, and concentrated under reduced pressure. The column chromatographic purification of crude mass on silica gel eluting with EtOAc-hexane provided 2-(3-Hydroxy-4-methoxyphenyl)-3-(3,4,5-trimethoxyphenylamino)imidazo[1,2-*a*]pyridine in 48% isolated yield.

(202 mg, 48%); Green solid; mp 170-172 °C; IR (KBr) ν_{max}/cm^{-1} 3310, 2933, 1607, 1504, 1438, 1231, 1010; δ_H (400 MHz; DMSO-d_6; Me_4Si) 3.63 (6 H, s), 3.67 (3 H, s), 3.87 (3 H, s), 5.87 (2 H, s), 6.92-6.97 (2 H, m), 7.36 (1 H, d, *J* 7.3), 7.46 (1 H, dd, *J* 1.8, *J* 8.4), 7.51 (1 H, d, *J* 1.8), 7.57 (1 H, d, *J* 9.0), 7.98 (1 H, d, *J* 6.8); δ_C(100 MHz, DMSO-d_6; Me_4Si) 56.3, 56.4, 61.3(OCH_3), 91.7, 112.6, 113.7, 115.2, 117.2, 119.8, 120.2, 124.3, 127.1, 127.3, 131.8, 139.7, 143.7, 143.8, 147.5, 149.2, 155.5; MS (APCI) *m/z* 422 ($M+H^+$); HRMS (ESI) Calcd for $C_{23}H_{23}N_3O_5Na$ $[M + Na]^+$ 444.1537, found *m/z* 444.1534.

All other compounds (**2**-**20**) were prepared following this reaction procedure. The structures of compounds were characterized by ^1H and ^{13}C NMR, IR and Mass (ESI or APCI) spectroscopies and confirmed by HRMS (ESI). The purity of the investigated compounds in HPLC were found to be >95%.

Biology

Cell line and culture conditions

The human embryonic kidney cancer cells (HEK 293T, cat. # CRL-11268), normal monkey kidney cells (Vero, cat. # CCL-81), breast cancer cells (MCF 7, cat. #HTB-22) and cervical

cancer cells SiHa (Cat# HTB-35) HeLA (Cat# CCL-2) were maintained in DMEM with 1% antibiotic (100 units of penicillin and 10 mg streptomycin per mL in 0.9% normal saline) and 10% fetal bovine serum in a humidified atmosphere in 5% CO_2 at 37 °C. Cell culture reagents were procured from Hi Media, Mumbai, India. All antibodies were purchased from Cell Signaling Technology (Danvers, MA, USA).

Tubulin assembly assay

To test the inhibitory activities of investigated compounds (**1**-**20**) for tubulin assembly formation, a protocol reported by Ducki et al.[76] and Lu et al.[90,91] with minor modification was followed. Instead of purified tubulin, cells lysate of HEK 293T cells were used. Briefly, exponentially growing cells were collected, washed once in PBS and lysed by adding RIPA lysis buffer on ice for 1 h. Then the cell lysate was centrifuged at 14,000 rpm for 5 min at 4 °C. The proteins estimation was done using Bradford's method. The samples were prepared by adding (35 µl) Mops buffer {[740 µl (0.1M Mops, 1mM EGTA, 0.5 mM $MgCl_2$, D/W, pH 6.6)], GTP (10 µl, 100 mM in Mops buffer)}. Lysate 40 µg protein and CA-4 or the investigated compounds of various concentrations were dissolved in DMSO with a final volume of 50 µl. The samples were immediately kept at 37 °C for 15 min and reaction was stopped in ice prior to measure optical density (O.D.) at 350 nm in spectrophotometer (EPOCH, USA). The results were compared to the untreated cells in order to evaluate the relative degree of change in the O.D. Data presented here in the tabular form is the best of three independent experiments.

Immunostaining of tubulin assembly

Immunostaining was carried out to detect microtubule associated tubulin protein after exposure to CA-4 and investigated compounds **1**, **2**, **14,** and **15**. Cells were seeded on coverslips and grown to 50-60% confluence. The HEK 293T cells were treated with LC_{50} concentrations of CA-4 and the investigated compounds for 24 h. The control and treated cells were fixed in acetone: methanol (1:1) for 20 min at -20 °C, washed with 1X PBS and were incubated for 30 min in 1X PBS containing 2% BSA, and 0.1% Triton X-100 for blocking. The primary tubulin antibody (Cell Signaling Technology, MA, USA) was diluted (1:1000) with 2% BSA in 1X PBS and incubated for 2 h at 37 °C. The cells were washed with 1X PBS to remove unbound primary antibody and then cells were incubated with FITC-conjugated anti-mouse secondary antibody (Imgenex, India), diluted (1:1000) with 2% BSA in PBS, for 1 h at room temperature. The cells were washed with 1X PBS to remove unbound secondary antibody, nucleus was stained with propidium iodide at a concentration of 10 µg/ml and then, immunofluorescence was detected using a Leica TCS SP5 confocal microscope. Data presented here is the best of three independent experiments.

MTT ASSAY

Cell proliferation of CA-4 and the investigated compounds (**1**-**20**) was measured by using a colorimetric assay [3-(4, 5-dimethylthiazol-2yl-)-2, 5-diphenyl tetrazolium bromide] (MTT), as described earlier.[63,92] Briefly, 8000-10,000 cells were seeded in a 96 well flat bottom tissue culture plates. After 24 h of incubation cells were exposed to compounds of different concentrations for different time point. After treatment, cells were washed with 1X PBS followed by addition of 100 µl of 0.05% MTT reagent to each well and overnight incubation at 37 °C. Purple color formazan crystals were formed and dissolved in detergent solution (10% NP-40 with 4 mM HCl). The mixture was incubated for 1 h in dark at RT. The color density was

measured spectrophotometrically at 570 nm using a microplate reader (Mithras LB 940 Multimode Microplate Reader, Berthold, Germany). The data was calculated and plotted as percent viability compared to control. Each data point was calculated in triplicate, and all assays were performed at least thrice.

Clonogenic cell survival assay

The clonogenic cell survival assay is a long-term cell viability assay that determines the ability of a single cell to proliferate indefinitely, thereby retaining its reproductive ability to form a colony or a clone. This assay was done to investigate the anti-colony-forming potential of compounds **1**, **2**, **14**, and **15** in kidney cancer cell lines (HEK 293) as compared to normal kidney epithelial cells (Vero) by the procedure described earlier.[92] Cells were seeded at approximately 500 cells per well in 12-well culture plate and kept for 24 h. Then they were treated with increasing concentrations of investigated compounds for another 48 h. Untreated plate was considered as control. After end of the treatment, medium was aspirated and replaced with fresh normal growth medium supplemented with 10% FBS, and cells were allowed to grow for 5-6 doublings. After every 3 days medium was aspirated and replaced with fresh medium. After end of the 5-6 doubling, the medium was removed and washed with 1X PBS. Then the plates were stained with 0.2% crystal violet for 1 h and excess dye was washed with distilled water. After air drying the plates, the colonies were counted using a gel documentation system (UVP, Germany). The colony in untreated plate considered as 100% survival. The percent survival was calculated by total number of colony in treated cells /total number of colony in untreated cells X 100. Experiments were conducted in triplicates, and the data were represented as percent survival (% control).

DAPI nuclear staining

Cellular apoptosis in HEK 293T cells, analysis of nuclear fragmentation as well as chromatin condensation was performed by DAPI nuclear staining.[93,94] 60-70% confluent cells were treated with LC_{50} concentrations of CA-4 and the compounds **1**, **2**, **14**, and **15** for 24 h. After treatment, cells were washed with ice-cold PBS followed by fixing with ice chilled acetone: methanol (1:1) for 10 min at -20 °C. The fixed cells were washed twice with chilled 1X PBS and incubated with DNA fluorochrome, DAPI solution for 1 h at 4 °C in the dark. Cells were washed with chilled 1X PBS to remove the excess stain and observed under fluorescence microscope (Nikon, Japan) at 40X magnification. Images presented are the best of three independent experiments.

Western blot analysis

The HEK 293T cells were grown in 100 mm tissue culture discs and cells were treated with LC_{50} concentrations of CA-4 and the investigated compounds **1**, **2**, **14**, and **15** for 24 h prior to harvest. The whole cell lysate was prepared by using modified RIPA lysis buffer and protein estimation was performed by Bradford's method.[95] The proteins were then separated in 10% SDS-PAGE and transferred on to polyvinylidene difluoride membranes. The membranes were immunoblotted with anti-p53 and anti-PARP antibodies according to the manufacturer's protocol. The anti-GAPDH was used as a control to access the loading of proteins. Blots shown here are the best of three experiments.

FACS analysis

The 60-70% confluent HEK 293T cells were treated with CA-4 and the investigated compounds **1**, **2**, **14**, and **15** for 24 h with their respective LC_{50} concentrations. At the end of the treatment an FACS analysis was carried out.[92] The DNA content was evaluated in a FACS scan flow cytometer (Becton Dickinson, CA) after staining the cells with propidium iodide (50 µg/ml) for

15 min at RT in the dark. For cell cycle analysis, the fluorescence emitted from single cell was quantified (10,000 cells/sample). The DNA content of the cells at different phases of cell cycle was determined by using Cell Quest Software (Becton and Dickinson, CA).

Single cell gel electrophoresis (SCGE) or comet assay

Comet assay was performed to measure the DNA damage and repair in the treated cells by a method described earlier.[92] The HEK 293T cells were exposed to CA-4 and the investigated compounds **1**, **2**, **14**, and **15** for 24 h prior to harvest. Approximately, 2000 cells were resuspended with 25 µl of 1X PBS and mixed with 75 µl of low melting agarose at 37 °C and then spread uniformly on a preheated (37 °C) comet slide. Further, the cells were processed according to the protocol and finally the SYBR green dye (40 µL) was added to air-dried slides and incubated in the dark for 30 min at room temperature to stain the DNA. The migration of DNA was observed using a fluorescence microscope (Nikon, Japan) at a magnification of 10X. Comet tail lengths were analyzed by TriTek CometScore™ software. Data were represented both by imaging and graphically by randomly selecting comet lengths of HEK 293T cells.

Cytokinesis-block micronucleus (CBMN) assay

To identify the micronuclei formation ability (chromosome damage) of investigated compounds **1**, **2**, **14**, and **15**, the established protocol of CBMN by Fenech et al. was followed.[75] The HEK 293T cells were grown in 6-well plate and treated with respectiveLC_{50} concentrations of CA-4 and its analogues for 24 h. After treatment, the cells were arrested at the cytokinesis stage by the addition of Cytochalasin-B (0.5 mg/ml) in 1X PBS at a concentration of 10 µg/ml and the cells were allowed to grow for 12 h. Afterwards, the cells were trypsinized and centrifuged at 1000 rpm for 10 min at RT. Cells were fixed by addition of ice cold methanol and acetic acid (3:1),

and incubated at 4 °C for 1 h. Finally few drops of cells suspension were added on slide, air-dried and stained with propidium iodide stain. The images were captured by Olympus BX61 fluorescence microscope using appropriate filters and analyzed by Cytovision 7.2 software.

Molecular Docking

Ligand Structure Preparation

The 3D structures of the synthesized 2-aryl-3-arylamino-imidazo-pyridines/pyrazines (compounds **1**-**20**) and known tubulin inhibitor, CA-4, were built using SYBYL 7.1[96] molecular modeling package installed on a Silicon Graphics Fuel Work station IRIX 6.5. The ligands were embedded with Gasteiger-Hückel partial charges[97]; energy minimization was then performed with Powell method using Tripos force field.[98] The default energy gradient convergence criterion of 0.05 kcal/mol was utilized during minimization. The optimized 3D structures of the ligands as well as extracted colchicine from PDB ID: 3UT5[99] were further submitted to LigPrep module of Maestro interface[83] using OPLS_2005 force field.[100] All possible low energy ionization, tautomeric and stereoisomeric states of ligands was generated within the range of pH 7.0 ± 2.0 (which corresponds to the physiological conditions).

Protein Structure Preparation

The 3D structure of human *α,β*-tubulin heterodimer is not determined either via X-ray crystallography or NMR spectroscopy till date; but about 11 X-ray crystal structures of the tubulin co-crystallized with inhibitor (bound at colchicine binding site) from other organisms (*Bos taurus* and *Ovis aries*) are available in Protein Data Bank (PDB). For the purpose of molecular docking studies, recently published X-ray crystal structure of *α,β*-tubulin heterodimer (PDB ID: 3UT5, resolution: 2.73 Å, organism *Ovis aries*)[99] was selected. This PDB ID is particularly chosen since it is available at a higher resolution without any missing structural

components and overall good B-factor as compared to other tubulin structures. Moreover, the sequence identity of α-subunit (Uniprot ID: Q71U36) and β-subunit (Uniprot ID: Q9BVA1) of *Homo sapiens* tubulin with the corresponding subunits of *Ovis aries* tubulin is 99.6% and 99.1% respectively, signifying high homology. Even these small differences are far from the colchicine binding site of tubulin.

The X-ray crystal structure of *Ovis aries* tubulin (PDB ID: 3UT5) is available in complex with inhibitors colchicine and ustiloxin D, cofactors GTP and GDP, and with the stathmin-like domain that plays a role in the regulation of microtubule assembly.[99] This PDB structure is composed of five chains, but for the present molecular docking study only two chains A and B were extracted *i.e.* α,β-heterodimer along with the bound ligand colchicine and cofactor GTP. Protein structure was prepared using Protein Preparation Wizard tool implemented in Maestro 9.3. The right bond orders were assigned, hydrogen atoms were added to the protein and all the water molecules were deleted. Protassign utility was employed for the optimization of hydroxyl group orientation, amide groups of Asn and Gln, and charged state of His residues. The final restrained minimization by the impref utility was performed with a cut-off point until the average RMSD of the hydrogen atoms reached 0.3 Å, leaving heavy atoms in place.

Grid Generation and GLIDE Docking

An interaction grid was generated around the colchicine binding site with the help of Receptor Grid Generation Wizard of GLIDE 5.7.[83,101,102] The centroid (xyz: 8.085, 55.861, 87.807) of the grid box was defined by selecting the bound ligand colchicine from the workspace and was extended up to 10 Å (size equivalent to the size of native ligand) from the center, with the outer

box extending an additional 24.71 Å. It was ensured that the dimensions of the grid box are long enough to completely cover the binding site cavity. Validation of docking protocol is a very crucial step for the extrapolation of docking results to the binding affinity. Therefore, the prepared extracted bound ligand (colchicine) was subjected to re-docking into the tubulin at Standard Precision mode using GLIDE 5.7.[102] Both the superimposed structures (bound and docked colchicine) showed similar interactions and binding pose at the binding site. This analysis establish the acceptability of docking protocol, which can be extended further to dock other ligands at the colchicine binding site of *α,β*-tubulin heterodimer.

After validation of the docking protocol, prepared ligands were docked at the interface of *α,β*-tubulin heterodimer following the same docking protocol using the OPLS_2005[100] force field. Number of poses generated for each ligand were set to 10 (while keeping all the parameters at their default values), and each one of them was critically evaluated for their binding mode, intermolecular interactions with the key residues of *α,β*-tubulin heterodimer and Glide docking score.[101]

Molecular Dynamics Simulations

MD simulations were performed on the best docking pose of the four potent investigated compounds (**1**, **2**, **14**, and **15**) and known tubulin inhibitor CA-4 with *α,β*-tubulin heterodimer using AMBER 11 package.[87] Amber ff99SB force field[103] was implemented for protein and General Amber Force Field (GAFF)[104] for ligands. RESP partial atomic charges[105] of ligands were derived at HF/6-31+G(d) level with the aid of GAUSSIAN03[84] and *antechamber*[106] module of AMBER. The protein structure with cofactor GTP and ligand was solvated using TIP3P water model,[107] solvent buffer being extended to 12 Å in each direction of the solute forming a cubical

box. The parameters of GTP (cofactor carrying -4 formal charges) were obtained from Bryce research group, Manchester University, UK (http://www.pharmacy.manchester.ac.uk/bryce/amber/). The system was neutralized by adding appropriate number of Na^+ ions (38 in case of CA-4 and 37 in case of other protonated ligands), followed by addition of 127 Na^+ and Cl^- ions to the system in order to mimic the physiological isotonicity by achieving the ionic concentration of 0.15 M NaCl. The specifics of the MD simulation protocol and binding free energy calculations using Molecular Mechanics-Generalized Born Surface Area (MM-GBSA) method[89] are given in supporting information.

ASSOCIATED CONTENT

Supporting Information. General experimental procedure; ^1H, ^{13}C, mass, IR, HRMS, and melting points for all investigated compounds (**1**-**20**), molecular docking results for all compounds (**1**-**20**) in their neutral and protonated states, quantum chemical calculations of potent compounds **1**, **2**, **14**, and **15** in their neutral and protonated states, binding pose of bound inhibitor colchicine at the interface of α,β-tubulin heterodimer, superimposition of bound (cyan) and docked (green) colchicine, superimposition of docked CA-4 and compound **2** on the bound inhibitor colchicine, and molecular dynamics simulation results. This material is available free of charge via the Internet at http://pubs.acs.org.

AUTHOR INFORMATION

Corresponding Authors*

For S.K.G.: phone, +91 (0)172 2214683; fax, +91 (0)172 2214692; E-mail, skguchhait@niper.ac.in. For C.N.K.: phone, +91 (0)674 2725466; fax, + 91 (0)674 2725732; E-mail, cnkundu@gmail.com.

ACKNOWLEDGMENTS

Authors gratefully acknowledge the financial support from Department of Science and Technology (DST), Indian Council of Medical Research (ICMR), Council of Scientific and Industrial Research (CSIR) and Department of Biotechnology (DBT), Government of India, New Delhi, for this investigation.

ABBREVIATIONS USED

CA-4: Combretastatin A-4

CBMN: Cytokinesis-block micronucleus

DAPI: 4′,6–diamidino–2–phenylindole

DFT: Density functional theory

FACS: Fluorescence activated cell sorter

GAFF: General amber force field

IC_{50}: Inhibitory concentration required to kill 50% of cell in culture

LC_{50}: Lethal concentration required to kill 50% of cell in culture

MTT: 3-(4,5-Dimethylthiazol-2yl-)-2,5-diphenyltetrazolium bromide

MD: Molecular dynamics

MM-GBSA: Molecular mechanics-generalized born surface area

PME: Particle-Mesh Ewald

PDB: Protein data bank

PARP: Poly (ADP-ribose) polymerase

RMSD: Root-mean-square deviation

3D: Three dimensional

References

1. R. Stephens and K. Edds, *Physiol. Rev.*, 1976, **56**, 709-777.
2. S. Etienne-Manneville, *Curr. Opin. Cell Biol.*, 2010, **22**, 104-111.
3. M. A. Jordan and L. Wilson, *Nat. Rev. Cancer*, 2004, **4**, 253-265.
4. Q. Li and H. L. Sham, *Expert Opin. Ther. Pat.*, 2002, **12**, 1663-1702.
5. M. Kavallaris, N. M. Verrills and B. T. Hill, *Drug Resist. Updat.*, 2001, **4**, 392-401.
6. C. M. Lin, H. H. Ho, G. R. Pettit and E. Hamel, *Biochemistry*, 1989, **28**, 6984-6991.
7. J. A. Hadfield, S. Ducki, N. Hirst and A. T. McGown, *Prog. Cell Cycle Res.*, 2003, **5**, 309-325.
8. F. Pellegrini and D. R. Budman, *Cancer Invest.*, 2005, **23**, 264-273.
9. G. M. Cragg and D. J. Newman, *J. Nat. Prod.*, 2004, **67**, 232-244.
10. E. Nogales, M. Whittaker, R. A. Milligan and K. H. Downing, *Cell*, 1999, **96**, 79-88.
11. R. B. Ravelli, B. Gigant, P. A. Curmi, I. Jourdain, S. Lachkar, A. Sobel and M. Knossow, *Nature*, 2004, **428**, 198-202.
12. S. B. Horwitz, *Trends Pharmacol. Sci.*, 1992, **13**, 134-136.
13. J. J. Manfredi and S. B. Horwitz, *Pharmacol. Ther.*, 1984, **25**, 83-125.
14. M. Jordan, *Curr. Med. Chem.: Anti-Cancer Agents*, 2002, **2**, 1-17.
15. G. R. Pettit, M. R. Rhodes, D. L. Herald, E. Hamel, J. M. Schmidt and R. K. Pettit, *J. Med. Chem.*, 2005, **48**, 4087-4099.
16. G. R. Pettit, S. B. Singh, M. L. Niven, E. Hamel and J. M. Schmidt, *J. Nat. Prod.*, 1987, **50**, 119-131.
17. A. Dorléans, B. Gigant, R. B. Ravelli, P. Mailliet, V. Mikol and M. Knossow, *Proc. Natl. Acad. Sci. U. S. A.*, 2009, **106**, 13775-13779.
18. G. Nagaiah and S. C. Remick, *Future Oncol.*, 2010, **6**, 1219-1228.
19. P. Hinnen and F. Eskens, *Br. J. Cancer*, 2007, **96**, 1159-1165.
20. M. J. McKeage and B. C. Baguley, *Cancer*, 2010, **116**, 1859-1871.
21. J. W. Lippert III, *Bioorg. Med. Chem.*, 2007, **15**, 605-615.
22. D. Patterson and G. Rustin, *Clin. Oncol.*, 2007, **19**, 443-456.
23. E. L. Schwartz, *Clin. Cancer Res.*, 2009, **15**, 2594-2601.
24. G. Tozer, C. Kanthou, G. Lewis, V. Prise, B. Vojnovic and S. Hill, *Br. J. Radiol.*, 2008, **81**, S12-S20.
25. B. C. Baguley and M. J. McKeage, *Clinical Investigation*, 2012, **2**, 985-993.
26. K. Ohsumi, R. Nakagawa, Y. Fukuda, T. Hatanaka, Y. Morinaga, Y. Nihei, K. Ohishi, Y. Suga, Y. Akiyama and T. Tsuji, *J. Med. Chem.*, 1998, **41**, 3022-3032.
27. A. Chaudhary, S. Pandeya, P. Kumar, P. Sharma, S. Gupta, N. Soni, K. Verma and G. Bhardwaj, *Mini Rev. Med. Chem.*, 2007, **7**, 1186-1205.
28. J. Chen, T. Liu, X. Dong and Y. Hu, *Mini Rev. Med. Chem.*, 2009, **9**, 1174-1190.
29. A. Gangjee, Y. Zhao, L. Lin, S. Raghavan, E. G. Roberts, A. L. Risinger, E. Hamel and S. L. Mooberry, *J. Med. Chem.*, 2010, **53**, 8116-8128.
30. G. C. Tron, T. Pirali, G. Sorba, F. Pagliai, S. Busacca and A. A. Genazzani, *J. Med. Chem.*, 2006, **49**, 3033-3044.
31. N.-H. Nam, *Curr. Med. Chem.*, 2003, **10**, 1697-1722.
32. D. Simoni, R. Romagnoli, R. Baruchello, R. Rondanin, M. Rizzi, M. G. Pavani, D. Alloatti, G. Giannini, M. Marcellini and T. Riccioni, *J. Med. Chem.*, 2006, **49**, 3143-3152.

33. L. Wang, K. W. Woods, Q. Li, K. J. Barr, R. W. McCroskey, S. M. Hannick, L. Gherke, R. B. Credo, Y.-H. Hui and K. Marsh, *J. Med. Chem.*, 2002, **45**, 1697-1711.
34. K. Odlo, J. Hentzen, S. Ducki, O. A. Gani, I. Sylte, M. Skrede, V. A. Fløtenes and T. V. Hansen, *Bioorg. Med. Chem.*, 2008, **16**, 4829-4838.
35. O. Provot, A. Hamze, J.-F. Peyrat, J.-D. Brion and M. Alami, *Anti-Cancer Agents in Medicinal Chemistry (Formerly Current Medicinal Chemistry-Anti-Cancer Agents)*, 2013, **13**, 1614-1635.
36. V. Jain, P. Saravanan, A. Arvind and C. G. Mohan, *Chem. Biol. Drug Des.*, 2011, **77**, 373-387.
37. V. K. Kretzschmann and R. Fürst, *Phytochem. Rev.*, 2013, 1-16.
38. N. H. Nam, *Curr. Med. Chem.*, 2003, **10**, 1697-1722.
39. K. G. Pinney, M. P. Mejia, V. M. Villalobos, B. E. Rosenquist, G. R. Pettit, P. Verdier-Pinard and E. Hamel, *Bioorg. Med. Chem.*, 2000, **8**, 2417-2425.
40. G. R. Pettit, J. W. Lippert, D. L. Herald, E. Hamel and R. K. Pettit, *J. Nat. Prod.*, 2000, **63**, 969-974.
41. A. Kamal, A. Mallareddy, M. J. Ramaiah, S. Pushpavalli, P. Suresh, C. Kishor, J. Murty, N. S. Rao, S. Ghosh and A. Addlagatta, *Eur. J. Med. Chem.*, 2012, **56** 166–178.
42. A. Hamze, E. Rasolofonjatovo, O. Provot, C. Mousset, D. Veau, J. Rodrigo, J. Bignon, J. M. Liu, J. Wdzieczak-Bakala and S. Thoret, *ChemMedChem*, 2011, **6**, 2179-2191.
43. M. Cushman, D. Nagarathnam, D. Gopal, H. M. He, C. M. Lin and E. Hamel, *J. Med. Chem.*, 1992, **35**, 2293-2306.
44. S.-M. Nathwani, L. Hughes, L. M. Greene, M. Carr, N. M. O'Boyle, S. McDonnell, M. J. Meegan and D. M. Zisterer, *Oncol. Rep.*, 2013, **29**, 585-594.
45. S. Aprile, E. Del Grosso, G. C. Tron and G. Grosa, *Drug Metab. Dispos.*, 2007, **35**, 2252-2261.
46. M. Cushman, D. Nagarathnam, D. Gopal, A. K. Chakraborti, C. M. Lin and E. Hamel, *J. Med. Chem.*, 1991, **34**, 2579-2588.
47. T. Hatanaka, K. Fujita, K. Ohsumi, R. Nakagawa, Y. Fukuda, Y. Nihei, Y. Suga, Y. Akiyama and T. Tsuji, *Bioorg. Med. Chem. Lett.*, 1998, **8**, 3371-3374.
48. Y. S. Shan, J. Zhang, Z. Liu, M. Wang and Y. Dong, *Curr. Med. Chem.*, 2011, **18**, 523-538.
49. B. L. Flynn, E. Hamel and M. K. Jung, *J. Med. Chem.*, 2002, **45**, 2670-2673.
50. B. L. Flynn, G. P. Flynn, E. Hamel and M. K. Jung, *Bioorg. Med. Chem. Lett.*, 2001, **11**, 2341-2343.
51. H. Chen, Y. Li, C. Sheng, Z. Lv, G. Dong, T. Wang, J. Liu, M. Zhang, L. Li and T. Zhang, *J. Med. Chem.*, 2013, **56**, 685-699.
52. A. B. Maya, C. Pérez-Melero, C. Mateo, D. Alonso, J. L. Fernández, C. Gajate, F. Mollinedo, R. Peláez, E. Caballero and M. Medarde, *J. Med. Chem.*, 2005, **48**, 556-568.
53. P. H. Jalily, J. A. Hadfield, N. Hirst and S. B. Rossington, *Bioorg. Med. Chem. Lett.*, 2012, **22**, 6731–6734.
54. L. M. Greene, S. Wang, N. M. O'Boyle, S. A. Bright, J. E. Reid, P. Kelly, M. J. Meegan and D. M. Zisterer, *Oncol. Rep.*, 2013, **29**, 2451-2458.
55. N. M. O'Boyle, L. M. Greene, N. O. Keely, S. Wang, T. S. Cotter, D. M. Zisterer and M. J. Meegan, *Eur. J. Med. Chem.*, 2013.

56. J. Aziz, E. Brachet, A. Hamze, J.-F. Peyrat, G. Bernadat, E. Morvan, J. Bignon, J. Wdzieczak-Bakala, D. Desravines and J. Dubois, *Org. Biomol. Chem.*, 2013, **11**, 430-442.
57. R. Álvarez, P. Puebla, J. F. Díaz, A. C. Bento, R. Garcia-Navas, J. de la Iglesia-Vicente, F. Mollinedo, J. M. Andreu, M. Medarde and R. Peláez, *J. Med. Chem.*, 2013, **56**, 2813-2827.
58. S. Kandekar, R. Preet, M. Kashyap, R. P. MU, P. Mohapatra, D. Das, S. R. Satapathy, S. Siddharth, V. Jain and M. Choudhuri, *ChemMedChem*, 2013, **8**, 1873–1884.
59. H. Rajak, P. Kumar Dewangan, V. Patel, D. Kumar Jain, A. Singh, R. Veerasamy, P. Chander Sharma and A. Dixit, *Curr. Pharm. Des.*, 2013, **19**, 1923-1955.
60. M. T. M. Mallinath B. Hadimani, Anjan Ghatak, Tracy E. Strecker, Ramona Lopez, Madhavi Sriram, Benson L. Nguyen, John J. Hall, Raymond J. Kessler, Anupama R. Shirali, Li Liu, Charles M. Garner, George R. Pettit, Ernest Hamel, David J. Chaplin , Ralph P. Mason, Mary Lynn Trawick, and Kevin G. Pinney, *J. Nat. Prod.*, 2013, **76**, 1668-1678.
61. A. Kamal, J. S. Reddy, M. J. Ramaiah, D. Dastagiri, E. V. Bharathi, M. V. P. Sagar, S. Pushpavalli, P. Ray and M. Pal-Bhadra, *MedChemComm*, 2010, **1**, 355-360.
62. K. G. Pinney, A. D. Bounds, K. M. Dingeman, V. P. Mocharla, G. R. Pettit, R. Bai and E. Hamel, *Bioorg. Med. Chem. Lett.*, 1999, **9**, 1081-1086.
63. A. T. Baviskar, C. Madaan, R. Preet, P. Mohapatra, V. Jain, A. Agarwal, S. K. Guchhait, C. N. Kundu, U. C. Banerjee and P. V. Bharatam, *J. Med. Chem.*, 2011, **54**, 5013-5030.
64. S. K. Guchhait and C. Madaan, *Synlett*, 2009, 628-632.
65. A. Kamal, V. S. Reddy, S. Karnewar, S. S. Chourasiya, A. B. Shaik, G. B. Kumar, C. Kishor, M. K. Reddy, M. Narasimha Rao and A. Nagabhushana, *ChemMedChem*, 2013, **8**, 2015-2025.
66. T. L. Nguyen, C. McGrath, A. R. Hermone, J. C. Burnett, D. W. Zaharevitz, B. W. Day, P. Wipf, E. Hamel and R. Gussio, *J. Med. Chem.*, 2005, **48**, 6107-6116.
67. A. McGown and B. Fox, *Anti-Cancer Drug Des.*, 1989, **3**, 249-254.
68. H. Bienayme and K. Bouzid, *Angew. Chem. Int. Ed.*, 1998, **37**, 2234-2237.
69. C. Blackburn, B. Guan, P. Fleming, K. Shiosaki and S. Tsai, *Tetrahedron Lett.*, 1998, **39**, 3635-3638.
70. K. Groebke, L. Weber and F. Mehlin, *Synlett*, 1998, 661-663.
71. S. K. Guchhait, C. Madaan and B. S. Thakkar, *Synthesis*, 2009, 3293-3300.
72. S. K. Guchhait and C. Madaan, *Org. Biomol. Chem.*, 2010, **8**, 3631-3634.
73. S. K. Guchhait, V. Chaudhary and C. Madaan, *Org. Biomol. Chem.*, 2012, **10**, 9271-9277.
74. S. K. Guchhait, G. Priyadarshani, V. Chaudhary, D. R. Seladiya, T. M. Shah and N. P. Bhogayta, *RSC Adv.*, 2013, **3**, 10867-10874.
75. M. Fenech, *Nat. Protoc.*, 2007, **2**, 1084-1104.
76. A. Massarotti, A. Coluccia, R. Silvestri, G. Sorba and A. Brancale, *ChemMedChem*, 2012, **7**, 33-42.
77. F. M. A. Bar, M. A. Khanfar, A. Y. Elnagar, F. A. Badria, A. M. Zaghloul, K. F. Ahmad, P. W. Sylvester and K. A. E. Sayed, *Bioorg. Med. Chem.*, 2010, **18**, 496-507.
78. C. Rappl, P. Barbier, V. Bourgarel-Rey, C. Grégoire, R. Gilli, M. Carre, S. Combes, J.-P. Finet and V. Peyrot, *Biochemistry*, 2006, **45**, 9210-9218.

79. G. De Martino, M. C. Edler, G. La Regina, A. Coluccia, M. C. Barbera, D. Barrow, R. I. Nicholson, G. Chiosis, A. Brancale and E. Hamel, *J. Med. Chem.*, 2006, **49**, 947-954.
80. F. Bellina, S. Cauteruccio, S. Monti and R. Rossi, *Bioorg. Med. Chem. Lett.*, 2006, **16**, 5757-5762.
81. N. D. Kim, E.-S. Park, Y. H. Kim, S. K. Moon, S. S. Lee, S. K. Ahn, D.-Y. Yu, K. T. No and K.-H. Kim, *Bioorg. Med. Chem.*, 2010, **18**, 7092-7100.
82. A. J. Knox, T. Price, M. Pawlak, G. Golfis, C. T. Flood, D. Fayne, D. C. Williams, M. J. Meegan and D. G. Lloyd, *J. Med. Chem.*, 2009, **52**, 2177-2180.
83. Maestro, version 9.3, Schrödinger, LLC, New York, 2012
84. M. J. Frisch, G. W. Trucks, H. B. Schlegel, G. E. Scuseria, M. A. Robb, J. R. Cheeseman, J. Montgomery, J. A.;, T. K. Vreven, K. N.;, J. C. Burant, J. M. Millam, S. S. Iyengar, J. Tomasi, V. Barone, B. Mennucci, M. Cossi, G. Scalmani, N. Rega, G. A. Petersson, H. Nakatsuji, M. Hada, M. Ehara, K. Toyota, R. Fukuda, J. Hasegawa, M. Ishida, T. Nakajima, Y. Honda, O. Kitao, H. Nakai, M. Klene, X. Li, J. E. Knox, H. P. Hratchian, J. B. Cross, V. Bakken, C. Adamo, J. Jaramillo, R. Gomperts, R. E. Stratmann, O. Yazyev, A. J. Austin, R. Cammi, C. Pomelli, J. W. Ochterski, P. Y. Ayala, K. Morokuma, G. A. Voth, P. Salvador, J. J. Dannenberg, V. G. Zakrzewski, S. Dapprich, A. D. Daniels, M. C. Strain, O. Farkas, D. K. Malick, A. D. Rabuck, K. Raghavachari, J. B. Foresman, J. V. Ortiz, Q. Cui, A. G. Baboul, S. Clifford, J. Cioslowski, B. B. Stefanov, G. Liu, A. Liashenko, P. Piskorz, I. Komaromi, R. L. Martin, D. J. Fox, T. Keith, M. A. Al-Laham, C. Y. Peng, A. Nanayakkara, M. Challacombe, P. M. W. Gill, B. Johnson, W. Chen, M. W. Wong, C. Gonzalez and J. A. Pople, Gaussian 03, Revision C.02, **2004**
85. MarvinView 5.2.3_1, 2009, ChemAxon (http://www.chemaxon.com/marvin),
86. G. La Regina, M. C. Edler, A. Brancale, S. Kandil, A. Coluccia, F. Piscitelli, E. Hamel, G. De Martino, R. Matesanz and J. F. Díaz, *J. Med. Chem.*, 2007, **50**, 2865-2874.
87. D. Case, T. Darden, T. Cheatham III, C. Simmerling, J. Wang, R. Duke, R. Luo, R. Walker, W. Zhang and K. Merz, AMBER 11, University of California, San Francisco, 2010
88. H. K. Srivastava and G. N. Sastry, *J. Chem. Inf. Model.*, 2012, **52**, 3088-3098.
89. P. A. Kollman, I. Massova, C. Reyes, B. Kuhn, S. Huo, L. Chong, M. Lee, T. Lee, Y. Duan and W. Wang, *Acc. Chem. Res.*, 2000, **33**, 889-897.
90. S. Ducki, G. Mackenzie, B. Greedy, S. Armitage, J. F. D. Chabert, E. Bennett, J. Nettles, J. P. Snyder and N. J. Lawrence, *Bioorg. Med. Chem.*, 2009, **17**, 7711-7722.
91. Y. Lu, C.-M. Li, Z. Wang, J. Chen, M. L. Mohler, W. Li, J. T. Dalton and D. D. Miller, *J. Med. Chem.*, 2011, **54**, 4678-4693.
92. R. Preet, P. Mohapatra, S. Mohanty, S. K. Sahu, T. Choudhuri, M. D. Wyatt and C. N. Kundu, *Int. J. Cancer*, 2012, **130**, 1660-1670.
93. F. Otto, *Methods Cell Biol.*, 1990, **33**, 105-110.
94. P. Mohapatra, R. Preet, M. Choudhuri, T. Choudhuri and C. N. Kundu, *Oncol. Res.*, 2011, **19**, 311-321.
95. N. J. Kruger, in *The protein protocols handbook*, Springer, 2009, pp. 17-24.
96. SYBYL7.1, Tripos International, 1699 South Hanley Rd., St. Louis, Missouri, 63144, USA,
97. J. Gasteiger and M. Marsili, *Tetrahedron*, 1980, **36**, 3219-3228.
98. M. J. D. Powell, *Mathematical programming*, 1977, **12**, 241-254.

99. F. M. Ranaivoson, B. Gigant, S. Berritt, M. Joullie and M. Knossow, *Acta Crystallogr., Sect. D: Biol. Crystallogr.*, 2012, **68**, 927-934.
100. W. L. Jorgensen, D. S. Maxwell and J. Tirado-Rives, *J. Am. Chem. Soc.*, 1996, **118**, 11225-11236.
101. R. A. Friesner, J. L. Banks, R. B. Murphy, T. A. Halgren, J. J. Klicic, D. T. Mainz, M. P. Repasky, E. H. Knoll, M. Shelley and J. K. Perry, *J. Med. Chem.*, 2004, **47**, 1739-1749.
102. Glide, version 5.7, Schrödinger, LLC New York, **2012**
103. V. Hornak, R. Abel, A. Okur, B. Strockbine, A. Roitberg and C. Simmerling, *Proteins: Struct., Funct., Bioinf.*, 2006, **65**, 712-725.
104. J. Wang, R. M. Wolf, J. W. Caldwell, P. A. Kollman and D. A. Case, *J. Comput. Chem.*, 2004, **25**, 1157-1174.
105. W. D. Cornell, P. Cieplak, C. I. Bayly and P. A. Kollmann, *J. Am. Chem. Soc.*, 1993, **115**, 9620-9631.
106. J. Wang, W. Wang, P. A. Kollman and D. A. Case, *J. Mol. Graph. Model.*, 2006, **25**, 247-260.
107. W. L. Jorgensen, J. Chandrasekhar, J. D. Madura, R. W. Impey and M. L. Klein, *J. Chem. Phys.*, 1983, **79**, 926-935.